

ENGINEERING OF BIOMATERIALS

INŻYNIERIA BIOMATERIAŁÓW

JOURNAL OF POLISH SOCIETY FOR BIOMATERIALS AND FACULTY OF MATERIALS SCIENCE AND CERAMICS AGH-UST

CZASOPISMO POLSKIEGO STOWARZYSZENIA BIOMATERIAŁÓW I WYDZIAŁU INŻYNIERII MATERIAŁOWEJ I CERAMIKI AGH

Number 165

Numer 165

Volume XXV

Rocznik XXV

Year 2022

(Issue 2)

Rok 2022

(Zeszyt 2)

ISSN 1429-7248

PUBLISHER:

WYDAWCA:

**Polish Society
for Biomaterials
in Krakow**

Polskie
Stowarzyszenie
Biomateriałów
w Krakowie

**EDITORIAL
COMMITTEE:**

KOMITET
REDAKCYJNY:

Editor-in-Chief

Redaktor naczelny

Elżbieta Pamuła

Editor

Redaktor

Patrycja

Domalik-Pyzik

Secretary of editorial

Sekretarz redakcji

Design

Projekt

Katarzyna Trała

**ADDRESS OF
EDITORIAL OFFICE:**

ADRES REDAKCJI:

AGH-UST

30/A3, Mickiewicz Av.

30-059 Krakow, Poland

Akademia

Górniczno-Hutnicza

al. Mickiewicza 30/A-3

30-059 Kraków

Issue: 250 copies

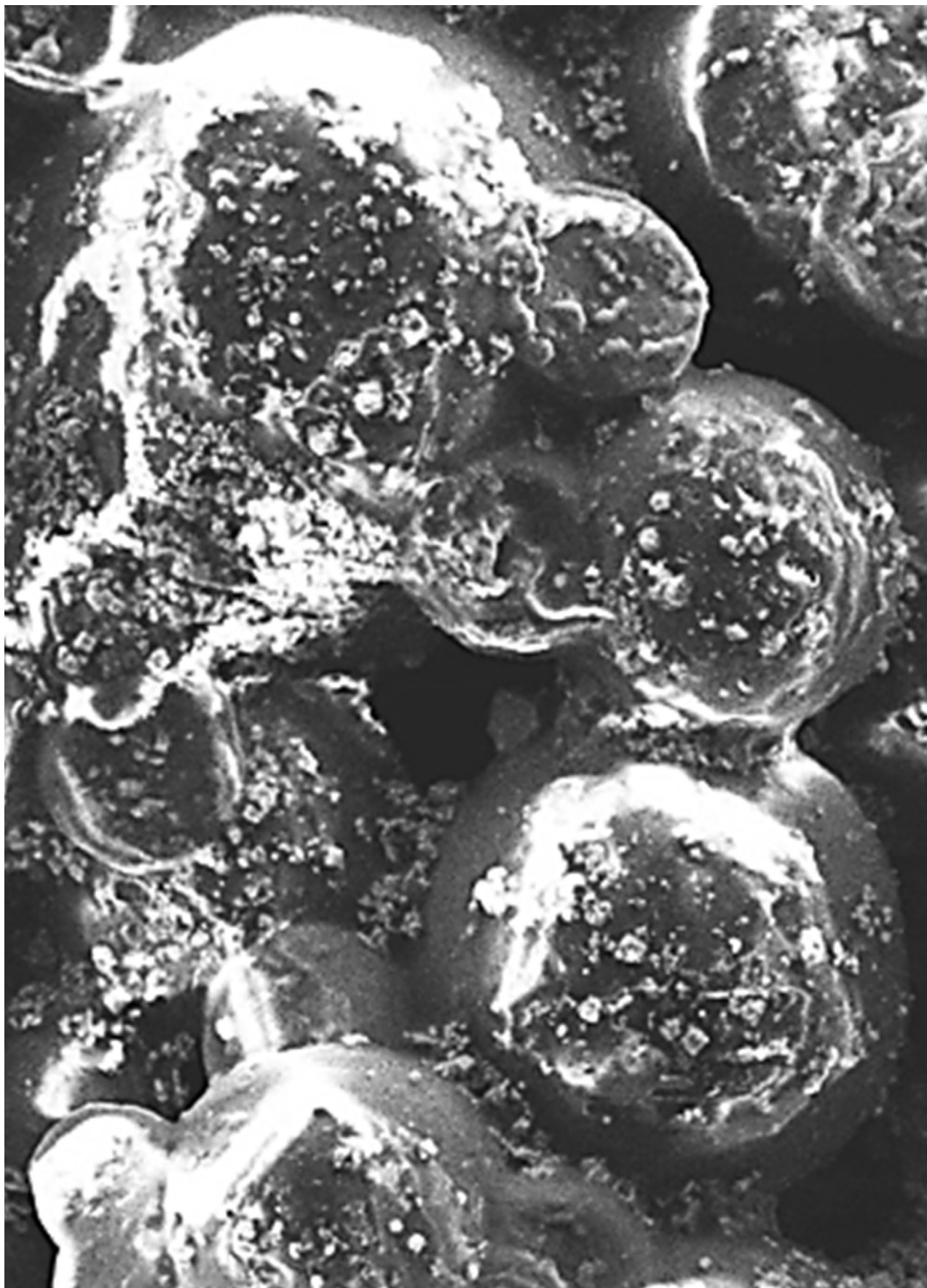
Nakład: 250 egz.

**Scientific Publishing
House AKAPIT**

Wydawnictwo Naukowe

AKAPIT

e-mail: wn@akapit.krakow.pl



**EDITORIAL BOARD
KOMITET REDAKCYJNY**

EDITOR-IN-CHIEF

Elżbieta Pamuła - AGH UNIVERSITY OF SCIENCE AND TECHNOLOGY, KRAKOW, POLAND

EDITOR

Patrycja Domalik-Pyzik - AGH UNIVERSITY OF SCIENCE AND TECHNOLOGY, KRAKOW, POLAND

**INTERNATIONAL EDITORIAL BOARD
MIĘDZYNARODOWY KOMITET REDAKCYJNY**

Iulian Antoniac - UNIVERSITY POLITEHNICA OF BUCHAREST, ROMANIA

Lucie Bacakova - ACADEMY OF SCIENCE OF THE CZECH REPUBLIC, PRAGUE, CZECH REPUBLIC

Romuald Będziński - UNIVERSITY OF ZIELONA GÓRA, POLAND

Marta Błażewicz - AGH UNIVERSITY OF SCIENCE AND TECHNOLOGY, KRAKOW, POLAND

Stanisław Błażewicz - AGH UNIVERSITY OF SCIENCE AND TECHNOLOGY, KRAKOW, POLAND

Wojciech Chrzanowski - UNIVERSITY OF SYDNEY, AUSTRALIA

Jan Ryszard Dąbrowski - BIAŁYSTOK TECHNICAL UNIVERSITY, POLAND

Timothy Douglas - LANCASTER UNIVERSITY, UNITED KINGDOM

Christine Dupont - UNIVERSITÉ CATHOLIQUE DE LOUVAIN, BELGIUM

Matthias Epple - UNIVERSITY OF DUISBURG-ESSEN, GERMANY

Robert Hurt - BROWN UNIVERSITY, PROVIDENCE, USA

James Kirkpatrick - JOHANNES GUTENBERG UNIVERSITY, MAINZ, GERMANY

Ireneusz Kotela - CENTRAL CLINICAL HOSPITAL OF THE MINISTRY OF THE INTERIOR AND ADMINISTR. IN WARSAW, POLAND

Małgorzata Lewandowska-Szumieł - MEDICAL UNIVERSITY OF WARSAW, POLAND

Jan Marciniak - SILESIA UNIVERSITY OF TECHNOLOGY, ZABRZE, POLAND

Ion N. Mihailescu - NATIONAL INSTITUTE FOR LASER, PLASMA AND RADIATION PHYSICS, BUCHAREST, ROMANIA

Sergey Mikhalovsky - UNIVERSITY OF BRIGHTON, UNITED KINGDOM

Stanisław Mitura - TECHNICAL UNIVERSITY OF LIBEREC, CZECH REPUBLIC

Piotr Niedzielski - TECHNICAL UNIVERSITY OF LODZ, POLAND

Abhay Pandit - NATIONAL UNIVERSITY OF IRELAND, GALWAY, IRELAND

Stanisław Pielka - WROCLAW MEDICAL UNIVERSITY, POLAND

Vehid Salih - UCL EASTMAN DENTAL INSTITUTE, LONDON, UNITED KINGDOM

Jacek Składzień - JAGIELLONIAN UNIVERSITY, COLLEGIUM MEDICUM, KRAKOW, POLAND

Andrei V. Stanishevsky - UNIVERSITY OF ALABAMA AT BIRMINGHAM, USA

Anna Ślósarczyk - AGH UNIVERSITY OF SCIENCE AND TECHNOLOGY, KRAKOW, POLAND

Tadeusz Trzaska - UNIVERSITY SCHOOL OF PHYSICAL EDUCATION, POZNAŃ, POLAND

Dimitris Tsipas - ARISTOTLE UNIVERSITY OF THESSALONIKI, GREECE

Wskazówki dla autorów

1. Prace do opublikowania w kwartalniku „Engineering of Biomaterials / Inżynieria Biomateriałów” przyjmowane będą wyłącznie w języku angielskim.

2. Wszystkie nadsyłane artykuły są recenzowane.

3. Materiały do druku prosimy przysyłać za pomocą systemu online (www.biomaterials.pl).

4. Struktura artykułu:

• TYTUŁ • Autorzy i instytucje • Streszczenie (200-250 słów) • Słowa kluczowe (4-6) • Wprowadzenie • Materiały i metody • Wyniki i dyskusja • Wnioski • Podziękowania • Piśmiennictwo

5. Autorzy przesyłają pełną wersję artykułu, łącznie z ilustracjami, tabelami, podpisami i literaturą w jednym pliku. Artykuł w tej formie przesyłany jest do recenzentów. Dodatkowo autorzy proszeni są o przesłanie materiałów ilustracyjnych (rysunki, schematy, fotografie, wykresy) w oddzielnych plikach (format np. .jpg, .gif., .tiff, .bmp). Rozdzielczość rysunków min. 300 dpi. Wszystkie rysunki i wykresy powinny być czarno-białe lub w odcieniach szarości i ponumerowane cyframi arabskimi. W tekście należy umieścić odnośniki do rysunków i tabel.

6. Na końcu artykułu należy podać wykaz piśmiennictwa w kolejności cytowania w tekście i kolejno ponumerowany.

7. Redakcja zastrzega sobie prawo wprowadzenia do opracowań autorskich zmian terminologicznych, poprawek redakcyjnych, stylistycznych, w celu dostosowania artykułu do norm przyjętych w naszym czasopiśmie. Zmiany i uzupełnienia merytoryczne będą dokonywane w uzgodnieniu z autorem.

8. Opinia lub uwagi recenzentów będą przekazywane Autorowi do ustosunkowania się. Nie dostarczenie poprawionego artykułu w terminie oznacza rezygnację Autora z publikacji pracy w naszym czasopiśmie.

9. Za publikację artykułów redakcja nie płaci honorarium autorskiego.

10. Adres redakcji:

Czasopismo

„Engineering of Biomaterials / Inżynieria Biomateriałów”

Akademia Górniczo-Hutnicza im. St. Staszica

Wydział Inżynierii Materiałowej i Ceramiki

al. Mickiewicza 30/A-3, 30-059 Kraków

tel. (48) 12 617 44 48, 12 617 25 61

e-mail: epamula@agh.edu.pl, kabe@agh.edu.pl

Szczegółowe informacje dotyczące przygotowania manuskryptu oraz procedury recenzowania dostępne są na stronie internetowej czasopisma:

www.biomaterials.pl

Instructions for authors

1. Papers for publication in quarterly journal „Engineering of Biomaterials / Inżynieria Biomateriałów” should be written in English.

2. All articles are reviewed.

3. Manuscripts should be submitted to editorial office through online submission system (www.biomaterials.pl).

4. A manuscript should be organized in the following order:

• TITLE • Authors and affiliations • Abstract (200-250 words) • Keywords (4-6) • Introduction • Materials and Methods • Results and Discussion • Conclusions • Acknowledgements • References

5. All illustrations, figures, tables, graphs etc. preferably in black and white or grey scale should be additionally sent as separate electronic files (format .jpg, .gif., .tiff, .bmp). High-resolution figures are required for publication, at least 300 dpi. All figures must be numbered in the order in which they appear in the paper and captioned below. They should be referenced in the text. The captions of all figures should be submitted on a separate sheet.

6. References should be listed at the end of the article. Number the references consecutively in the order in which they are first mentioned in the text.

7. The Editors reserve the right to improve manuscripts on grammar and style and to modify the manuscripts to fit in with the style of the journal. If extensive alterations are required, the manuscript will be returned to the authors for revision.

8. Opinion or notes of reviewers will be transferred to the author. If the corrected article will not be supplied on time, it means that the author has resigned from publication of work in our journal.

9. Editorial does not pay author honorarium for publication of article.

10. Address of editorial office:

Journal

„Engineering of Biomaterials / Inżynieria Biomateriałów”

AGH University of Science and Technology

Faculty of Materials Science and Ceramics

30/A-3, Mickiewicz Av., 30-059 Krakow, Poland

tel. (48) 12) 617 44 48, 12 617 25 61

e-mail: epamula@agh.edu.pl, kabe@agh.edu.pl

Detailed information concerning manuscript preparation and review process are available at the journal's website:

www.biomaterials.pl



31st Biomaterials in Medicine and Veterinary Medicine Annual Conference

13 – 16 October 2022 Rytro, Poland

SAVE THE DATE

13-16

OCTOBER
2022

www.biomat.agh.edu.pl



REGISTER
AND
SUBMIT
AN ABSTRACT



SPIS TREŚCI CONTENTS

SURFACE MODIFICATIONS OF BIOMATERIAL WITH DIFFERENT COLD PLASMA REACTORS TO IMPROVE CELL ADHESION
 PIOTR TEREKUN, MICHAŁ WÓJCIK,
 MARTA TRZASKOWSKA, MICHAŁ KWIATKOWSKI,
 DAWID ZARZECZNY, PAULINA KAZIMIERCZAK,
 JOANNA PAWŁAT, AGATA PRZEKORA **2**

OPTIMIZATION OF THE PREPARATION PROCESS STAGES OF THE BIOINK COMPOSITIONS BASED ON SODIUM ALGINATE AND GELATIN TO IMPROVE THE VIABILITY OF BIOLOGICAL MATERIAL CONTAINED IN HYDROGEL 3D PRINTOUTS
 ADRIANNA WIERZBICKA, MATEUSZ BARTNIAK,
 KAROLINA ROSIŃSKA, DOROTA BOCIĄGA **7**

BIOLOGICAL AND MECHANICAL RESEARCH OF TITANIUM IMPLANTS COVERED WITH BACTERICIDAL COATING
 KLAUDIA MALISZ, BEATA ŚWIECZKO-ŻUREK **17**

EXPERIMENTAL INVESTIGATIONS OF THE PMMA BONE CEMENT DISTRIBUTION INSIDE A MODEL OF LUMBAR VERTEBRAE
 ARTUR BONIK, ZBIGNIEW TYFA,
 LECHOSŁAW F. CIUPIK, KRZYSZTOF SOB CZAK,
 AGNIESZKA KIERZKOWSKA, DAMIAN OBIDOWSKI,
 DARIUSZ WITKOWSKI, TOMASZ PAŁCZYŃSKI,
 MARCIN ELGALAL, PIOTR KOMOROWSKI,
 EDWARD SŁOŃSKI, KRZYSZTOF JÓZWIK,
 BOGDAN WALKOWIAK **23**

SURFACE MODIFICATIONS OF BIOMATERIAL WITH DIFFERENT COLD PLASMA REACTORS TO IMPROVE CELL ADHESION

PIOTR TEREKUN¹ , MICHAŁ WÓJCIK² ,
MARTA TRZASKOWSKA² , MICHAŁ KWIATKOWSKI¹ ,
DAWID ZARZECZNY¹ , PAULINA KAZIMIERCZAK² ,
JOANNA PAWŁAT¹ , AGATA PRZEKORA^{2*} 

¹ INSTITUTE OF ELECTRICAL ENGINEERING AND ELECTROTECHNOLOGIES, LUBLIN UNIVERSITY OF TECHNOLOGY, NADBYSTRZYCKA 38A, 20-618 LUBLIN, POLAND

² INDEPENDENT UNIT OF TISSUE ENGINEERING AND REGENERATIVE MEDICINE, MEDICAL UNIVERSITY OF LUBLIN, CHODZKI 1 STR., 20-093 LUBLIN, POLAND

*E-MAIL: AGATA.PRZEKORA@UMLUB.PL

Abstract

There is a growing trend in the engineering of biomaterials, focusing on surface modifications of biomaterials to improve their mechanical strength, corrosion resistance, and biological properties. Cold plasma treatment may improve biological properties of biomaterials for biomedical applications by enhancing their integration with host tissue. This study investigated the influence of different cold plasma treatments on the surface properties of a polysaccharides-based biomaterial to improve cell adhesion to its surface. The samples were subjected to plasma treatment using three different reactors operating at atmospheric pressure: gliding arc discharge (GAD) reactor, dielectric barrier discharge (DBD) plasma jet, and DBD surface reactor. Next, surface chemistry of the biomaterial after plasma treatment was determined by ATR-FTIR analysis. Furthermore, a cell adhesion assay on the samples was carried out using normal human skin fibroblasts (BJ cell line). The attenuated total reflection Fourier transform infrared analysis (ATR-FTIR) showed that new potential functional groups could be formed on the material surface after plasma treatment. However, plasma treatment of the samples did not enhance cell adhesion to the surface of the polysaccharides-based biomaterial. Thus, the obtained results indicate that plasma treatment using GAD reactor, DBD plasma jet, and DBD surface reactor was not effective for surface modification and cell responses.

Keywords: curdlan, agarose, gliding arc discharge reactor, dielectric barrier discharge plasma jet, dielectric barrier discharge surface reactor, surface modification

Introduction

Nowadays, there is a growing trend in the engineering of biomaterials that focuses on surface modifications to improve mechanical strength, corrosion resistance, and biological properties of the implants, e.g. to increase cell adhesion and proliferation and reduce the risk of infection after implantation [1,2]. Surface roughness, wettability, surface chemistry, and charge are among the factors that influence cell adhesion [2,3]. Moreover, strong adhesion is crucial for rapid cell proliferation and migration on the surface of biomaterials used as potential implants [3]. It was proven that polar and positively charged surfaces provide the most effective adsorption of protein to the surface of biomaterials, allowing good cell adhesion. For instance, Keselowsky et al. reported that the adhesion of cells to surfaces with differently chargeable functional groups followed the trend: OH > COOH = NH₂ > CH₃, by modulating fibronectin adsorption and direct integrin binding of cells to the fibronectin [3,4]. Plasma techniques are well-established technologies commonly used to modify the chemistry and topography of the biomaterials for different applications to improve their biocompatibility and interactions with tissues. Plasma techniques may be classified into two main classes: thermal plasma that is used mainly as a surface coating technology and low-temperature plasma that is used to directly treat living tissues [1,2]. Electric plasmas depending on the used substrate gas, allow formation of highly reactive species, such as ions, electrons, photons, free radicals, etc., which may further react with the treated material [5,6].

The aim of this work was to evaluate the impact of different cold plasma treatments, using 3 reactors operating at atmospheric pressure: gliding arc discharge (GAD) reactor, dielectric barrier discharge (DBD) plasma jet, and DBD surface reactor, on the improvement of the surface of biomaterials to increase cell adhesion. In the study, a polysaccharides-based biomaterial containing curdlan and agarose was used, whose surface has previously been proven to be unsupportive to cell adhesion [7]. After the plasma treatment, the surface chemistry of the biomaterial was assessed by ATR-FTIR. Moreover, the evaluation of cell viability and adhesion to the surface of plasma-treated biomaterial was performed.

Materials and Methods

Preparation of biomaterial

The biomaterial composition was previously optimized to achieve the most desired microstructural and physicochemical properties. The resultant curdlan/agarose biomaterial and method for its production were claimed in the Polish Patent no. 236367 (2021). Briefly, the biomaterial was prepared by suspending 2% (w/v) curdlan (Wako Pure Chemicals Industries, Japan) and 2% (w/v) agarose (Sigma-Aldrich Chemicals, Poland) in deionized water. The suspension was then transferred to round-shaped flat molds, which were placed in a water bath at a temperature of 95°C for 20 min, and then the resultant biomaterials were cooled and frozen at -80°C for 24 hours. The frozen samples were lyophilized for 18 h under medium vacuum of 6 x 10⁻² mbar (LYO GT2-Basic, SRK Systemtechnik GmbH, Riedstadt, Germany).

[Engineering of Biomaterials 165 (2022) 2-6]

doi:10.34821/eng.biomat.165.2022.2-6

Submitted: 2022-09-23, Accepted: 2022-10-12, Published: 2022-10-28



Copyright © 2022 by the authors. Some rights reserved.
Except otherwise noted, this work is licensed under
<https://creativecommons.org/licenses/by/4.0>

Plasma generator and plasma treatment of the surface of biomaterials

The plasma treatment was performed using three reactors operating at atmospheric pressure: gliding arc discharge (GAD) reactor, dielectric barrier discharge (DBD) plasma jet, and DBD surface reactor. Their operating parameters are summarized in TABLE 1, and the discharge geometry is presented in FIG. 1. For each reactor, 3 series of repetitions were performed for the treatment times of 30, 120 and 300 s. The treatment time and distance were selected as the most promising on the basis of the former research work using DBD and GAD reactors [5,8].

Surface chemistry analysis of biomaterial after plasma treatment

In the ATR-FTIR study on the identification of bonds after plasma treatment, a FT-IR-4200 type A (Jasco, Tokyo, Japan) spectrometer with ATR PRO ONE (Jasco, Tokyo, Japan) single reflection attachment with ZnSe crystal was used. The measurements were taken immediately after the treatment, using a set screw with a torque limiter.

Evaluation of cell viability and adhesion to the surface of biomaterials after plasma treatment

Cell culture experiments were performed using normal human skin fibroblasts (BJ cell line) obtained from the American Type Culture Collection (ATCC-LGC Standards). The BJ cells were incubated at 37°C in a humidified atmosphere (95%) with 5% carbon dioxide content and maintained in Eagle's Minimum Essential Medium (EMEM, ATCC-LGC Standards, Teddington, UK) with 10% fetal bovine serum (Pan-Biotech GmbH, Aidenbach, Bavaria, Germany), and 1% penicillin-streptomycin solution (Sigma-Aldrich Chemicals, Poland).

Before the experiment, the cube-shaped biomaterials (3 mm x 3 mm x 3 mm) were placed in 48-well plates and preincubated overnight in 300 µl of the EMEM complete culture medium. Then, 1×10^5 BJ cells (at passage 6) were seeded on the biomaterials in the 500 µl culture medium and cultured at 37°C for 48 hours. To evaluate cell viability and adhesion to the surface of biomaterials, the BJ cells were stained using Live/Dead Double Staining Kit (Sigma-Aldrich Chemicals, Poland) and visualized using a confocal laser scanning microscope (CLSM, Olympus Fluoview equipped with FV1000, Olympus, Japan).

TABLE 1. Characteristics of plasma reactors.

Type	Max. voltage	Mean power	Frequency	Working gas	Geometry
GAD	3.7 kV	40 W	50 Hz	Forced nitrogen flow (440 lph)	Sample placed perpendicular to the gas stream, 2 cm from the electrodes.
Surface DBD	3.7 kV	10 W	17 kHz	Air	Sample placed at a distance of 2 cm from the electrode, in a 37 dm ³ glass cubic container.
DBD plasma jet	3.7 kV	6 W	17 kHz	Forced flow of a mixture containing helium (100 lph) and nitrogen (1 lph)	Sample placed perpendicular to the gas stream, 3 cm from the end of ceramic tube

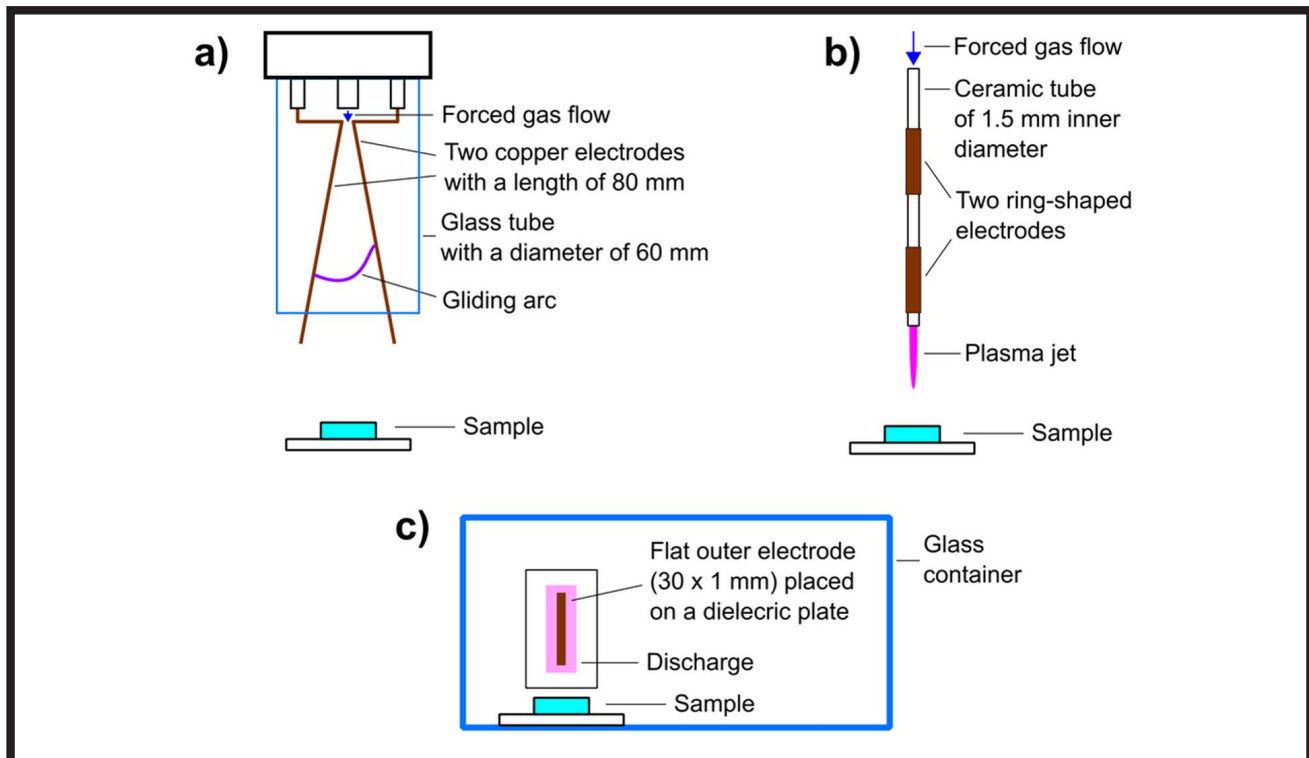


FIG. 1. Schematic diagrams of the atmospheric plasma treatment systems: (a) GAD reactor; (b) DBD plasma jet; (c) surface DBD.

Results and Discussions

Physicochemical analysis of the surface of biomaterials after plasma treatment

The ATR-FTIR analysis was carried out for carbon and nitrogen bond matching. The presented results were characterized by a low value of the signal to noise ratio, which, combined with the presence of many other peaks in the studied areas, did not allow to clearly indicate the exact formation of permanent bonds. The noticeable changes caused by plasma treatment were best seen for the band in the range from 1300 to 1900 cm^{-1} , where peaks characteristic for ketones (bands 1710-1720, 1680-1700, 1715-1810 cm^{-1}) and nitro compounds (bands 1500-1600, 1300-1390 cm^{-1}) were observed (FIG. 2). Peaks associated to C=O stretching (potentially of ketones or amides) around 1640 and 1680 cm^{-1} ; N-H bending of amines around 1650 and 1340 cm^{-1} and some peaks associated with both symmetrical and asymmetrical N-O stretching around 1583 and 1350 cm^{-1} could be noticed. The measurements were carried out just after the plasma treatment and changes in spectra appeared for all the tested cases, including reactors and treatment times (FIG. 2), in comparison to the untreated material. As expected, the absorbance value increased with the treatment time. The highest absorbance values indicating potential formation of new functional groups, which might improve biocompatibility of plasma treated material were obtained for the materials treated with the surface DBD reactor. The absorbance value for the mentioned peaks was on average 58% higher than the GAD reactor and 157% higher than the DBD plasma jet. Unfortunately, such high absorbance did not find reflection during the evaluation of cell viability and adhesion to the surface, which may suggest that the 300 s treatment time was too short to allow the formation of permanent bonds. Moreover, some secondary reactions could take place during the transportation and preservation of samples, which effected in further regrouping, leading to the loss of surface functionalization. Thus, further investigations employing changing of plasma treatment parameters are planned.

Evaluation of cell viability and adhesion to the surface of biomaterials after plasma treatment

Polysaccharides are often used in various tissue engineering applications for the production of implants or artificial organs. Natural polymers, such as curdlan (linear bacterial β -1,3-glucan) and agarose, are characterized by high biocompatibility, biodegradability, and wide availability making them widely used in biomaterials engineering [9]. In our previous research [7], a curdlan/agarose biomaterial was developed which was characterized by non-cytotoxicity and a foam-like structure with superabsorbent ability. Moreover, the surface of the fabricated biomaterial was unfavourable for cell adhesion. In this study, the cold plasma treatment of the developed biomaterial using different reactors was performed to improve cell adhesion to its surface. As shown in FIG. 3, the plasma treatments of the surface of polysaccharides-based biomaterial did not improve cell adhesion.

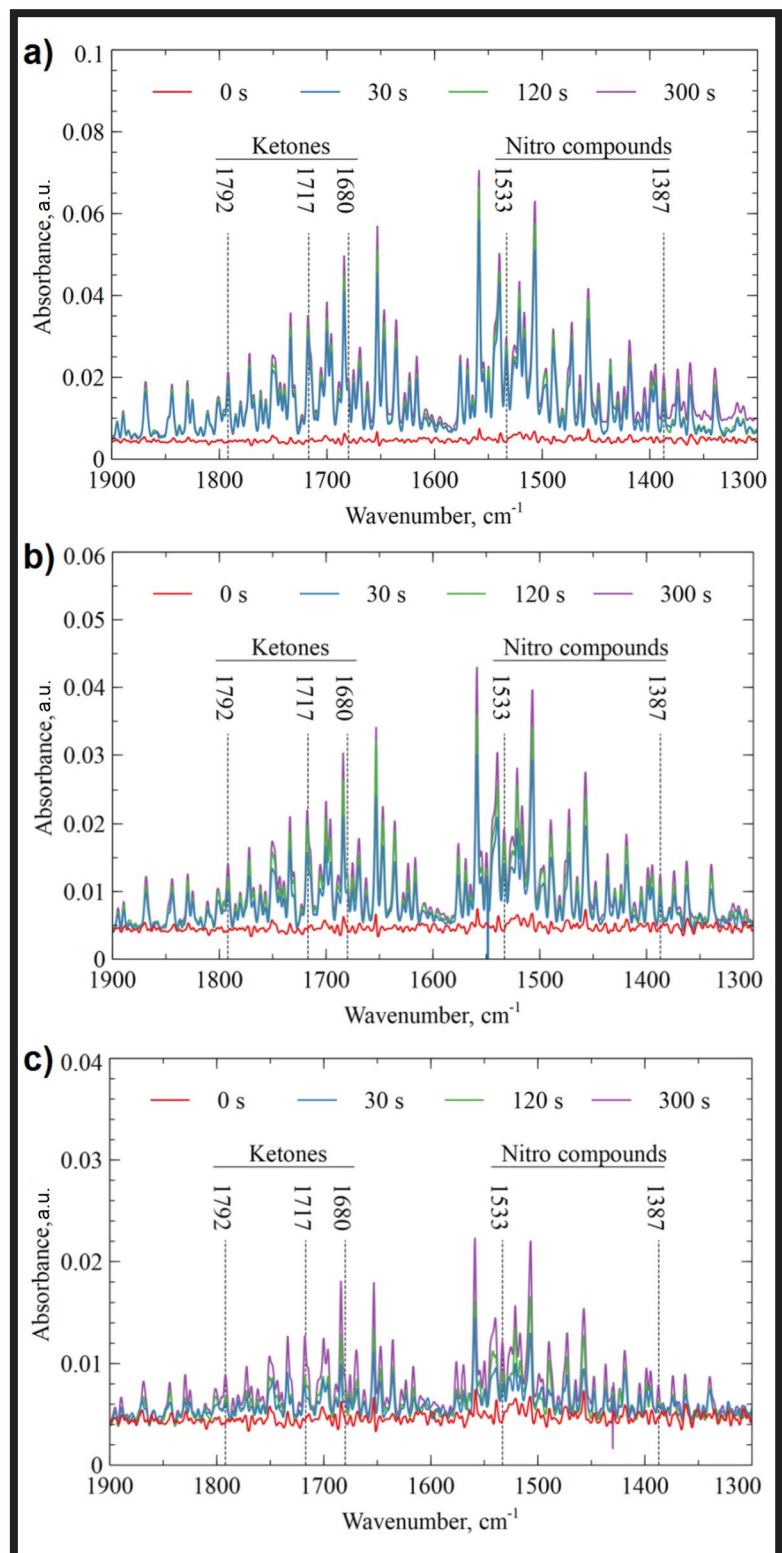


FIG. 2. ATR-FTIR spectra of the curdlan/agarose biomaterials after different plasma treatment times with (a) the DBD surface reactor, (b) the GAD reactor, and (c) the DBD plasma jet reactor.

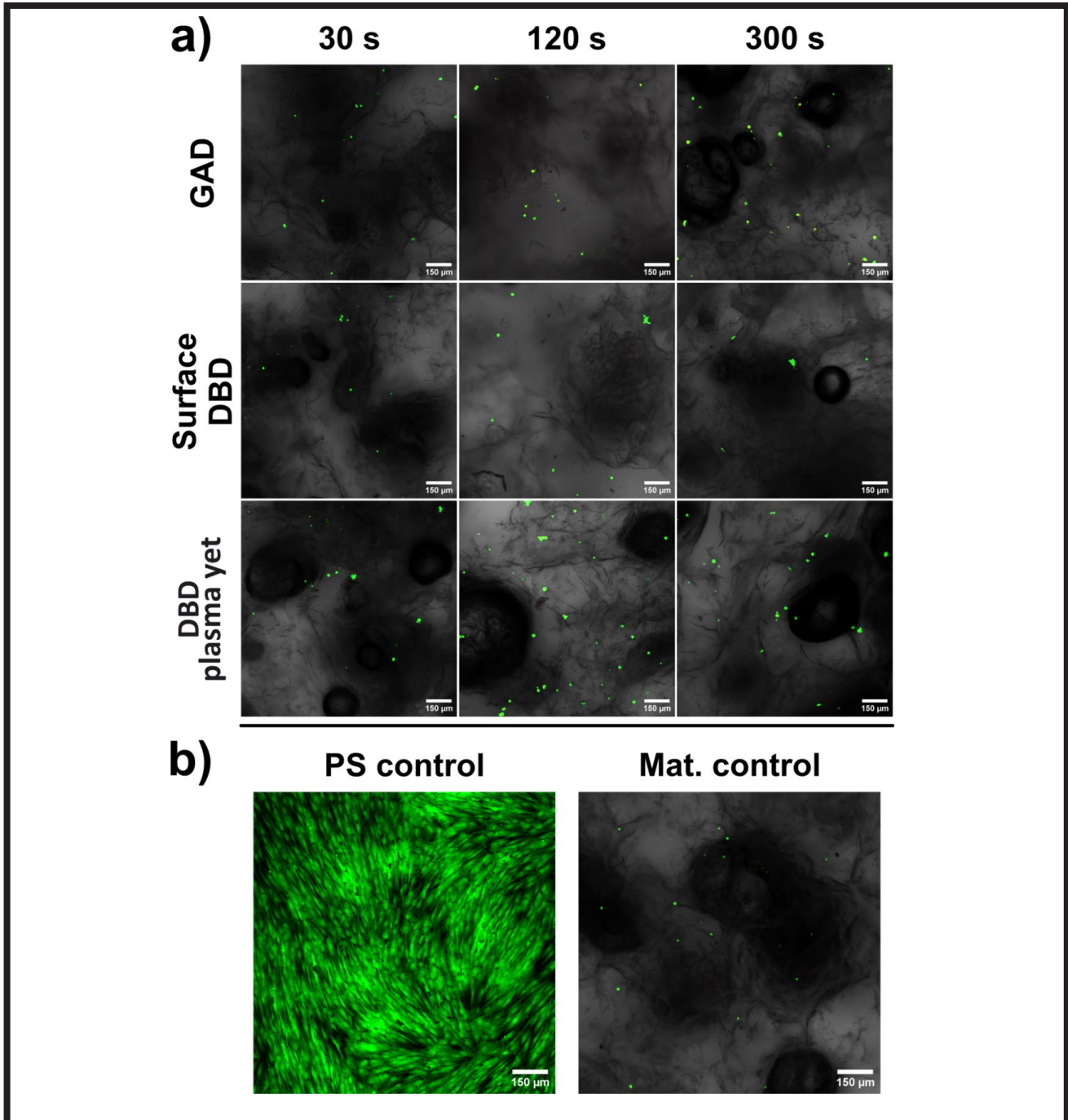


FIG. 3. Evaluation of cell viability and adhesion to the surface of (a) plasma-treated biomaterials and (b) non-treated biomaterial (Mat. Control) by Live/Dead double fluorescent staining and confocal laser scanning microscope visualization (PS control – control cells cultured on the surface of polystyrene well of multiwell plate; viable cells – green fluorescence; dead cells – red fluorescence; magnification 100x, scale bar = 150 μm).

The results obtained with Live/Dead staining of BJ cells cultured on the surface of biomaterials after the plasma treatment showed that the cells were viable (only green fluorescence was detected), but had a round shape, meaning that surfaces of biomaterials did not support cell attachment and adhesion. The extended plasma treatment times (from 30 to 300 s) were not effective for improvement of cell responses either. Moreover, there were no differences between the morphology of the cells cultured on the surface of the plasma-treated biomaterials and the non-treated control biomaterial (Mat. control).

Conclusions

Plasma treatment is widely used to improve cell interactions with polymer surfaces used in biomedical applications [10-12]. In this study, it was proven that the plasma treatment of the curdlan/agarose biomaterial using GAD reactor, DBD plasma jet, and DBD surface reactor was not effective for the surface modification and cell responses. Human fibroblasts cultured on the surface of biomaterials after plasma treatment had a round shape, indicating that the biomaterial surface did not support cell adhesion. Thus, further studies are needed to find an efficient plasma method that will improve cell adhesion to the curdlan/agarose biomaterial.

Acknowledgments

This research was funded by the National Science Centre (NCN) in Poland within OPUS 16 grant no. UMO-2018/31/B/ST8/00945. The research was partially supported by the Ministry of Education and Science in Poland within the statutory activity of the Medical University of Lublin (DS3/2022 project).

ORCID iD

P. Terebun: <https://orcid.org/0000-0002-3947-9552>
 M. Wójcik: <https://orcid.org/0000-0002-1918-6912>
 M. Trzaskowska: <https://orcid.org/0000-0001-6360-6702>
 M. Kwiatkowski: <https://orcid.org/0000-0001-5697-3176>
 D. Zarzeczny: <https://orcid.org/0000-0003-2029-9962>
 P. Kazimierzczak: <https://orcid.org/0000-0002-5893-7168>
 J. Pawlat: <https://orcid.org/0000-0001-8224-0355>
 A. Przekora: <https://orcid.org/0000-0002-6076-1309>

References

- [1] Kazimierzczak P., Przekora A.: Osteoconductive and osteoinductive surface modifications of biomaterials for bone regeneration: A concise review. *Coatings* 10(10) (2020) 971. doi:10.3390/coatings10100971
- [2] Yan M., Hartjen P., Gosau M., et al.: Effects of a novel cold atmospheric plasma treatment of titanium on the proliferation and adhesion behavior of fibroblasts. *Int J Mol Sci.* 23(1) (2022) doi:10.3390/ijms23010420
- [3] Przekora A.: The summary of the most important cell-biomaterial interactions that need to be considered during in vitro biocompatibility testing of bone scaffolds for tissue engineering applications. *Mater Sci Eng C.* 97 (2019) 1036-1051. doi:10.1016/j.msec.2019.01.061
- [4] Keselowsky B.G., Collard D.M., Garcia A.J.: Surface chemistry modulates fibronectin conformation and directs integrin binding and specificity to control cell adhesion. *J Biomed Mater Res Part A.* 66(2) (2003) 247-259. doi:10.1002/jbm.a.10537
- [5] Pawlat J., Terebun P., Kwiatkowski M., et al.: Evaluation of oxidative species in gaseous and liquid phase generated by mini -gliding arc discharge. *Plasma Chem Plasma Process.* 39(3) (2019) 627-642. doi:10.1007/s11090-019-09974-9
- [6] Przekora A., Audemar M., Pawlat J., et al.: Positive effect of cold atmospheric nitrogen plasma on the behavior of mesenchymal stem cells cultured on a bone scaffold containing iron oxide-loaded silica nanoparticles catalyst. *Int J Mol Sci.* 21 (2020) 4738. doi:10.3390/ijms21134738
- [7] Wójcik M., Kazimierzczak P., Benko A., Palka K., Vivcharenko V., Przekora A.: Superabsorbent curdlan-based foam dressings with typical hydrocolloids properties for highly exuding wound management. *Mater Sci Eng C* 124 (2021) 112068. doi:10.1016/j.msec.2021.112068
- [8] Kwiatkowski M., Terebun P., Mazurek P., Pawlat J.: Wettability of polymeric materials after dielectric barrier discharge atmospheric-pressure plasma jet treatment. *Sensors Mater.* 30(5) (2018) 1207-1212. doi:10.18494/SAM.2018.1890
- [9] Zarrintaj P., Manouchehri S., Ahmadi Z., et al.: Agarose-based biomaterials for tissue engineering. *Carbohydr Polym.* 187 (2018) 66-84. doi:10.1016/j.carbpol.2018.01.060
- [10] Liu C., Bai J., Wang Y., et al.: The effects of three cold plasma treatments on the osteogenic activity and antibacterial property of PEEK. *Dent Mater.* 37(1) (2021) 81-93. doi:10.1016/j.dental.2020.10.007
- [11] Teraoka F., Nakagawa M., Hara M.: Surface modification of poly(L-lactide) by atmospheric pressure plasma treatment and cell response. *Dent Mater J.* 25(3) (2006) 560-565. doi:10.4012/dmj.25.560
- [12] Hage M., Khelissa S., Akoum H., Chihib N.E., Jama C.: Cold plasma surface treatments to prevent biofilm formation in food industries and medical sectors. *Appl Microbiol Biotechnol.* 106(1) (2022) 81-100. doi:10.1007/s00253-021-11715-y

OPTIMIZATION OF THE PREPARATION PROCESS STAGES OF THE BIOINK COMPOSITIONS BASED ON SODIUM ALGINATE AND GELATIN TO IMPROVE THE VIABILITY OF BIOLOGICAL MATERIAL CONTAINED IN HYDROGEL 3D PRINTOUTS

ADRIANNA WIERZBICKA , MATEUSZ BARTNIAK ,
KAROLINA ROSIŃSKA , DOROTA BOCIĄGA* 

FACULTY OF MECHANICAL ENGINEERING,
INSTITUTE OF MATERIALS SCIENCE AND ENGINEERING,
LODZ UNIVERSITY OF TECHNOLOGY,
STEFANOWSKIEGO STR. 1/15, 90-537 LODZ, POLAND
*E-MAIL: DOROTA.BOCIAGA@P.LODZ.PL

Abstract

Currently developing on a large scale, the opportunities for 3D printing represent more and more perspective solutions in the area of tissue engineering and personalized medicine. Due to their ability to reproduce the natural extracellular matrix and unique properties, hydrogels are popularly used materials to produce bioinks designated for 3D printing. Today, solutions based on sodium alginate and gelatin are frequently used compositions for this purpose. The high viability of the cells incorporated into bioink is the key parameter determining the application opportunities of printed structures. The parameters of the process used for the preparation of hydrogel compositions may have a direct impact on the viability of the cells incorporated within the printed structure. This study aims to develop a protocol for the preparation of hydrogel materials based on alginate and gelatin, providing the highest viability of the model osteoblast-like cell line Saos-2 incorporated directly into the bioink before the 3D bioprinting process. In the scope of this study, the analyzed process parameters of the preparation of the hydrogel bioinks are the method of combination of a polymer solution with biological material, the applied concentration, the cross-linking solution, and also the waiting time of the prepared hydrogel bioink for the 3D printing process. A key aspect of the study is the evaluation of the influence of 3D printing on changes in the survival rate of biological material directly after the manufacturing process and after individual incubation periods of the printouts in conditions reflecting the body's environment.

Keywords: hydrogel, bioink, 3D bioprinting, sodium alginate, gelatin, tissue engineering

[Engineering of Biomaterials 165 (2022) 7-16]

doi:10.34821/eng.biomat.165.2022.7-16

Submitted: 2022-09-27, Accepted: 2022-11-21, Published: 2022-11-30



Copyright © 2022 by the authors. Some rights reserved.
Except otherwise noted, this work is licensed under
<https://creativecommons.org/licenses/by/4.0>

Introduction

Regarding the application of hydrogel materials, they represent a highly versatile group of materials, which currently finds a wide range of applications, including biomedicine. The beginning of clinical applications of hydrogels came in the 60s of the last century, when these materials were characterized and described by O. Wichterle and D. Lim as materials used for the construction of contact and intraocular lenses [1-4]. Literature data show that hydrogels represent the first polymer biomaterials designed for clinical applications [4]. According to the definition, a hydrogel is described as a network of hydrophilic polymers forming a three-dimensional structure. The presence of hydrophilic functional groups results in the ability of this group of materials for the reversible process of absorption of vast amounts of water. The cross-linking of the hydrogels results in the fact that despite the absorption of large amounts of fluids and the swelling ability, they maintain their geometry [1,2]. In general, hydrogel materials are also characterized by high flexibility, porosity, and the possibility of response to external stimuli [5]. Currently, the literature describes numerous methods of hydrogel classification. The most commonly used factors that allow for systematic division of this group of materials are origin, polymer composition, degree of crystallinity, network electrical charge, cross-linking type, macroscopic evaluation, and degradation ability [1,2,5,6].

Due to their properties, hydrogel materials can provide an extremely beneficial environment for cell cultures in a 3D arrangement. Their biocompatibility, high fluid absorption, and the possibility of adjusting mechanical properties for the requirements of various applications mean that these materials can provide conditions close to the natural extracellular matrix [7]. The 3D printing capabilities expanding on a large scale create increasingly promising solutions for tissue engineering and personalized medicine. Additive manufacturing methods can be applied to form biomimetic constructs, which provide a perspective to design complete tissues and organs of the body [8]. We can distinguish several 3D printing techniques, among which the most commonly applied are extrusion-based printing, inkjet, laser printing, and stereolithography [9-11]. In general, as inks in 3D bioprinting techniques, hydrogel bioinks are used, consisting of polymer solution and biological material incorporated in it. Due to the possibility of applying a wide range of various polymer solutions with different viscosities as well as the application of high-density biological material, including cell aggregates, the 3D bioprinting technique based on extrusion of bioink is currently gaining high popularity [10,11]. Commonly applied materials for bioink production are hydrogels based on sodium alginate. It is a natural anionic polysaccharide consisting of linked residues (1-4)-linked β -D-mannuronic acid (M) and its C-5 epimer α -1-guluronic acid (G) [11,12]. Depending on the contents of G, M, and GM blocks, the physical properties of alginate may undergo modulation [13]. Due to the presence of G-blocks, the alginate has the ability to form gels, whereby through the presence of M and GM blocks, this biopolymer is characterized by flexibility [11]. Alginate undergoes ionic cross-linking, during which interactions between divalent cations, such as Ca^{2+} , Ba^{2+} , Mn^{2+} , Sr^{2+} , Zn^{2+} , and Mg^{2+} , and free carboxyl groups occur [14,15]. Alginate hydrogels are characterized by high biocompatibility, water and gas permeability, and mild conditions of gelation. They undergo limited, frequently uncontrolled degradation processes in the physiological environment. Those hydrogels can be modified to obtain desired properties designated for particular applications [15,16].

An important property of alginate-based hydrogels is the possibility of modifying the rheological properties, making them attractive materials used to produce hydrogel bioinks for tissue engineering. However, alginate hydrogels lack groups that stimulate the adhesion and proliferation of the cells in their structure, which results in their biological inertness [7,16,17]. To eliminate the disadvantages of alginate related to the lack of the biological groups binding cells in the hydrogel bioinks, its combination with the addition of gelatin is often used. It provides biocompatible, biodegradable protein obtained during the collagen hydrolysis process. Gelatin contains in its structure bioactive sequences of RGD collagen (arginine–glycine–aspartic acid), which actively promotes adhesion and the growth of the cells incorporated into the hydrogel [7, 17-19]. Gelatin undergoes a sol-gel transition reaction during cooling in the range of temperatures of 20-30°C, which is a kind of thermo-reversible physical cross-linking [19]. The rheological properties of alginate- and gelatin-based hydrogels at room temperature make these materials ideal substrates for bioinks applied in additive technologies because they minimize the risk of damage to the cells incorporated into the bioink during the bioprinting process [7]. In order to achieve high viability and promote the proliferation of the cells encapsulated in a hydrogel bioink based on the polymer solutions mentioned above, it is recommended to apply lower alginate concentrations, which can form soft gels [18,20].

Important aspects of printability using a designed hydrogel bioink are shape compatibility, resolution, biocompatibility of the bioink, and the ability for cellular stimulation [13]. Designing and selecting appropriate physical properties of alginate-based hydrogels for particular applications is possible by analyzing available cross-linking methods, application of molecules with different chemical structures, or by change of cross-linking functionality [21]. The method and parameters used in the preparation process of alginate- and gelatin-based hydrogel bioinks may directly influence the quality of the obtained print and the viability of the cells incorporated into its structure. Before the bioprinting process, optimizing the individual stages of preparation of the hydrogel bioinks designated to be combined with the biological material is essential. The high viability of the cells incorporated into the volume of the hydrogel bioink and the printed structures are the key factors determining the application possibilities of the discussed material.

This study aims to perform an analysis of the influence of different parameters of the hydrogel preparation process of bioinks based on the selected composition of sodium alginate and gelatin (2% w/v alginate and 9% w/v gelatin) containing model osteoblast-like cell line *Saos-2*. The research conducted aims to develop a protocol of alginate-gelatin bioinks preparation, ensuring the highest cell viability of the model line contained in the polymer solutions directly before the 3D bioprinting process. A key aspect of this study is to evaluate the influence of 3D printing on the viability of biological material directly after the manufacturing process and to analyse the changes in cell survival rate in the printouts after individual periods of their incubation under conditions reflecting the body environment.

Materials and Methods

In the present work, the effect of the preparation method of hydrogel composition based on sodium alginate (Alg) and gelatin (Gel), methods of combining them with biological material, the type of cross-linking solution based on calcium chloride, and its concentration on the survival rate of the *Saos-2* line cells contained inside the material were analysed. The cell survival rate was also assessed as a function of the length of waiting time of prepared hydrogel bioink for the 3D printing process. The final component of the study was to evaluate the effect of the 3D printing process on changes in the survival rate of the biological material during subsequent incubation periods of the printouts under standard conditions, i.e., the temperature of 37°C, at 100% relative humidity, in 5% carbon dioxide and 95% of the air.

Materials

A hydrogel material composition containing 2% w/v sodium salts of alginic acid (Alg) from brown algae (Sigma Aldrich, USA) and 9% w/v gelatin (Gel) from porcine skin type B (Sigma Aldrich, USA) was used in the study. The hydrogel solutions were prepared in the McCoy's 5A culture medium (Capricorn Scientific GmbH, Germany) supplemented with 15% of FBS (Fetal Bovine Serum) (Sigma Aldrich, USA) and 1% of P/S (Penicillin/Streptomycin Solution) (Capricorn Scientific GmbH, Germany). Each time before the preparation process of the hydrogel solutions, appropriate amounts of sodium alginate and gelatin powders underwent UV sterilization for 1 hour. Calcium chloride (Sigma Aldrich, USA) was used for cross-linking the polymer solutions. After the cross-linking process, the samples were rinsed with PBS buffer (Phosphate-Buffered Saline) (Capricorn Scientific GmbH, Germany). Cell survival rate was assessed using live/dead staining (Biotium, CA, USA).

Cell viability assessment through live/dead assay

For the preparation of the hydrogel bioinks model line of immortalized *Saos-2* osteoblast-like cells (ATCC, USA) was used. The cultivation was conducted using complete McCoy's 5A culture medium (Capricorn Scientific GmbH, Germany) supplemented with 15% of FBS (Fetal Bovine Serum) (Sigma Aldrich, USA) and 1% P/S (Penicillin/Streptomycin Solution) (Capricorn Scientific GmbH, Germany) in an incubator under standard conditions. Cell passages were performed after 70-80% confluence was achieved.

The analysis of cell viability in bioinks and hydrogel printouts was carried out with live/dead staining using the mixture of dyes: calcein-AM applied for green labeling of live cells and ethidium homodimer (EthD) responsible for red labeling of dead cells. The cells incorporated in bioinks and hydrogel printouts were imaged using a fluorescent microscope (Nikon Eclipse LV100ND, Tokyo, Japan). The images of live and dead cells were taken in 10 randomly chosen areas of the analyzed samples. Based on the recorded images, the number of live and dead cells was calculated using ImageJ (LOCI, University of Wisconsin, USA). To determine the viability of the *Saos-2* line cells, the following relation was used:

$$\text{Viability [\%]} = \frac{\text{the number of living cells}}{\text{the number of living cells} + \text{dead cells}} \cdot 100\%$$

The results presented in the following sections show the calculated average viability of the cells incorporated into bioinks or hydrogel printouts.

Hydrogels preparation

Optimization of the cross-linking solution - selection of the concentration of the cross-linking solution based on CaCl_2 and the type of solvent used for its preparation

Sodium alginate and gelatin were dissolved independently in McCoy's 5A culture medium dedicated to Saos-2 line cells with the addition of 15% FBS and 1% P/S for 1 hour at a temperature of 37°C with the speed of 150 rpm to obtain solutions with concentrations of 4% w/v Alg and 18% w/v Gel. The prepared polymer solutions were combined in a 1:1 ratio, obtaining a composition of 2% w/v Alg and 9% w/v Gel. The obtained binary polymer solution was combined directly with Saos-2 line cell pellet. The biological material was stirred with the polymer composition for 1 min using a serological pipette with a capacity of 25 ml. The density of biological material in the hydrogel solution was $1 \cdot 10^6$ cells/ml. The hydrogel bioink prepared this way was poured onto 24-well plates forming samples of equal height (FIG. 1). The samples were cross-linked with various calcium chloride solutions, as shown in TABLE 1. The cross-linking time of each of the samples was 10 min. The cross-linking process was carried out at room temperature. After the cross-linking process, each sample was rinsed with PBS buffer three times. The evaluation of cell survival rate in hydrogel bioinks directly after the individual processes of cross-linking and rinsing of the samples was carried out using the live/dead assay.



FIG. 1. An example picture of alginate- and gelatin-based hydrogel bioinks placed on 24-well plates.

TABLE 1. Compositions and concentrations of used cross-linking CaCl_2 -based solutions.

The solvent used to prepare CaCl_2 cross-linking solution	CaCl_2 concentration
Deionized water	0.75%
Deionized water	1.5%
Deionized water	5%
McCoy's 5A	0.75%
McCoy's 5A	1.5%
McCoy's 5A	5%

Optimizing the method of combining alginate-gelatin solutions with the cell pellet

Three separate solutions of hydrogels were prepared in a volume ratio by mixing alginate and gelatin powders simultaneously in McCoy's 5A culture medium dedicated to Saos-2 line cells with the addition of 15% FBS and 1% P/S for 1 hour at a temperature of 37°C at a speed of 150 rpm.

The following methods of combining the cell pellet with hydrogel material were analyzed:

- a direct combination of the hydrogel with the cell pellet,
- the initial combination of the cell pellet with 2% of the volume of culture medium used to prepare the hydrogel, followed by a combination of the cell suspension with the hydrogel material,
- the initial combination of the cell pellet with 8% of the volume of culture medium used to prepare the hydrogel, followed by a combination of the cell suspension with hydrogel materials.

The obtained binary polymer solutions were combined directly with the cell pellet or the corresponding cell suspensions of the Saos-2 line according to the data given in TABLE 2. The biological material was stirred for 1 min with the alginate-gelatin solution using a serological pipette of 25 ml capacity. The obtained density of biological material in the hydrogel bioink was $1 \cdot 10^6$ cells/ml.

TABLE 2. Tested methods of combining biological material with the polymer solution.

The amount of culture medium subtracted initially from the prepared hydrogel	The composition of the hydrogel mixture used
0%	1 g Alg + 4.5 g Gel + 50 ml McCoy's 5A
2%	1 g Alg + 4.5 g Gel + 49 ml McCoy's 5A
8%	1 g Alg + 4.5 g Gel + 46 ml McCoy's 5A

The prepared hydrogel bioinks were poured onto 24-well plates forming samples of equal height (analogous to FIG. 1). Each sample was cross-linked using the 5% CaCl_2 solution prepared in McCoy's 5A culture medium. The cross-linking time of each of the samples was 10 min. The cross-linking process was carried out at room temperature. After the cross-linking process, each sample was rinsed in PBS buffer three times. Assessment of the cell survival rate in hydrogel materials directly after individual cross-linking and rinsing processes of the samples was carried out using the live/dead assay.

Evaluation of rheological properties of polymer solution containing 2%Alg 9%Gel (w/v) intended for 3D printing process

According to the results of the preceding studies, which have allowed us to select the bioink preparation method providing the highest cell survival rate, a polymer solution with a final concentration of 2%Alg 9%Gel in a volume ratio was prepared by mixing together alginate and gelatin powders, initially subtracting 8% of the culture medium from the mixture, which finally was added to the cell pellet of the Saos-2 line. Polymer solution was mixed at a temperature of 37°C with a speed of 150 rpm for 1 hour. The rheological properties of the polymer solution prepared in an optimized method were evaluated using an MCR502 rheometer (Anton Paar, Graz, Austria). For the measurement, a parallel plate geometry with a diameter of 20 mm was used. The viscosity test was conducted at 34°C, which is analogous to the conditions of the 3D bioprinting process. The measurement was carried out in the shear rate range of 1-1000 1/s. Before the test, the prepared polymer solution was thermostated for 10 min to achieve an even temperature of the material in the entire volume.

The effect of bioink waiting time for 3D printing and evaluation of the effect of the 3D bioprinting process itself on the viability of the cells contained in hydrogel printouts

An appropriate amount of the hydrogel providing a seeding density equal to $1 \cdot 10^6$ cells/ml was added to the cell suspension. The biological material was mixed with the polymer composition described in the previous section using a serological pipette with a capacity of 25 ml. The prepared bioink was divided into three parts, which were placed in separate sterile syringes with a capacity of 5 ml. Two parts of the bioink were subjected to incubation under standard conditions for respective time periods - 30 and 45 min before the printing process. The bioink not subjected to the incubation process was the reference - it was used to make the printouts right after combining the hydrogel with the biological material. The prepared hydrogel bioinks were used for direct printing of tube structures, which were divided using a surgical scalpel into identical samples with a length of 5 mm and inner diameter of 6 mm (FIG. 2A-C).

The 3D bioprinting process was performed using an own design bioprinter (FIG. 3) in which the material is pneumatically extruded, and the printing takes place on the horizontal shaft using the cone nozzle. The set print height refers to the final wall thickness of the obtained tubular structure. The height of the print layer was set to $250 \mu\text{m}$. During the 3D bioprinting process, the prepared bioink was heated up to the temperature of 34°C .

The printed samples were cross-linked using a 5% CaCl_2 solution prepared in McCoy's 5A culture medium. The cross-linking time of each of the samples was 10 min. The cross-linking process was carried out at room temperature. After the cross-linking process, each sample was rinsed with PBS buffer three times. The viability assessment of the cells contained in the printouts was carried out using the live/dead assay.

The effect of incubation time of 3D printouts on the viability of the cells contained in them

The polymer solution with a final concentration of 2% Alg 9%Gel was prepared in a volume ratio by mixing together sodium alginate and gelatin, initially subtracting 8% of the culture medium from the mixture, which subsequently was used to suspend the cell pellet. The alginate-gelatin solution was mixed at a temperature of 37°C with a speed of 150 rpm for 1 h. The missing amount of McCoy's 5A medium was added to the Saos-2 line cell pellet. An appropriate amount of the hydrogel providing a seeding density equal to $1 \cdot 10^6$ cells/ml was added to the cell suspension. The biological material was stirred for 1 min with the polymer composition using a serological pipette of 25 ml capacity. The prepared hydrogel bioink was used for direct printing of structures in the form of tubes, which were divided using a surgical scalpel into identical samples (analogously to the process of preparation of the printouts described in previous section). Each sample was cross-linked using the 5% CaCl_2 solution prepared in McCoy's 5A culture medium. The cross-linking time was 10 min. The cross-linking process was carried out at room temperature. After the cross-linking process, each sample was rinsed in PBS buffer three times. The printouts were placed in 24-well plates supplemented with 1.5 ml of McCoy's 5A culture medium + 15% FBS + 1% P/S and subjected to respective periods of incubation of 1 and 3 days under standard conditions. The assessment of the viability of the cells contained in printouts directly after the manufacturing process and after each incubation period was carried out using the live/dead assay.

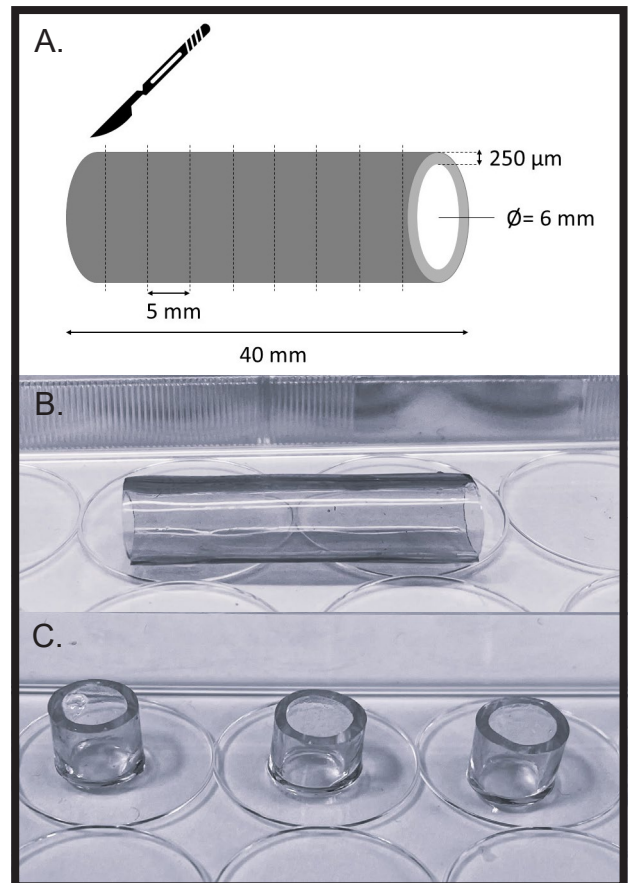


FIG. 2. A. Schematic of preparation of the hydrogel printouts samples; B. Example picture of a single hydrogel printout; C. Photo of samples obtained by cutting the hydrogel printout.

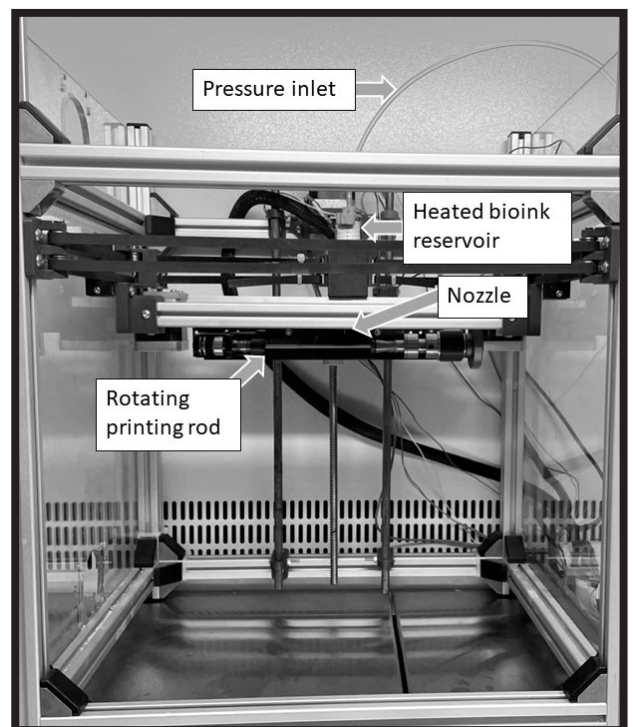


FIG. 3. A picture of a 3D bioprinter of own design which was used to print samples.

Statistical analysis

Each experiment was carried out in three repetitions for each sample. The results of survival rates are presented as mean \pm standard deviation. Statistical significance was assessed using a one-way ANOVA analysis of variance. Statistical significance was marked in the graphs with an asterisk when $p < 0.05$.

Results and Discussion

Hydrogels preparation

Results of optimization of the cross-linking solution - selection of a concentration of CaCl_2 -based cross-linking solution and the type of solvent used for its preparation

The test results of the effect of the concentration of the CaCl_2 -based cross-linking solution and the type of solvent used for its preparation are presented in FIG. 4. The study showed that the hydrogel samples cross-linked with CaCl_2 solutions prepared in McCoy's 5A culture medium are characterized by a higher survival rate of the Saos-2 line cells compared to the hydrogels cross-linked with aqueous CaCl_2 solutions. The highest cell survival rate, equal to $88.2 \pm 2.0\%$, is observed for hydrogels cross-linked with 0.75% CaCl_2 solution in culture medium and hydrogels cross-linked with 5% CaCl_2 solution prepared in culture medium ($88.0 \pm 2.1\%$). The lowest survival rate is observed for the samples cross-linked with a 5% aqueous CaCl_2 solution, for which the cell viability is $76.6 \pm 1.4\%$. According to ISO standard 10993 - Part 5 [22], materials that do not demonstrate cytotoxic effects are considered those for which the cell viability reaches the value of $\geq 70\%$. Thus, for all the materials analyzed, biocompatibility was obtained. Calcium ions are used in eukaryotic cell culture. They are essential for the normal function of vital cells. Literature data indicate that the endoplasmic reticulum stores calcium, but a low calcium concentration (2 mM) is required in the cytoplasm to maintain normal cellular functions [23]. The use of higher concentrations of calcium chloride extracellularly can lead to osmotic stress, due to disruption of cellular electrolytes, resulting in cell membrane damage [23-25]. However, the degree of cellular destruction varies, depending on the used concentration of calcium ions and the duration of exposure of the biological material to their action. Damage of cells may preserve their functional activity and proliferative capacity for regeneration or damage them completely. The applied calcium ion concentration should balance the osmotic stress. The study conducted by N. Cao's team and collaborators indicated that the rate of cell proliferation is higher in hydrogels with high calcium concentrations, which may be a result of calcium ion exchange, which is an important second transmitter signal in cell metabolism, between cells and their extracellular environments [23]. Research conducted by the L. Fischer team demonstrated that the physiological concentration of calcium ions in the hydrogel can increase cell survival after 3D bioprinting, because they can improve the ability of cells to overcome shear stress-induced deformation and plasma membrane damage during the extrusion process [26]. Higher concentrations of the cross-linking solution allow for obtaining a more stable structure of the gel by the increased availability of ions cross-linking the material. Higher Ca^{2+} concentrations are responsible for the formation of gels with higher cross-linking densities. The mechanical properties of alginate hydrogels are mainly controlled by the cross-linking density [27].

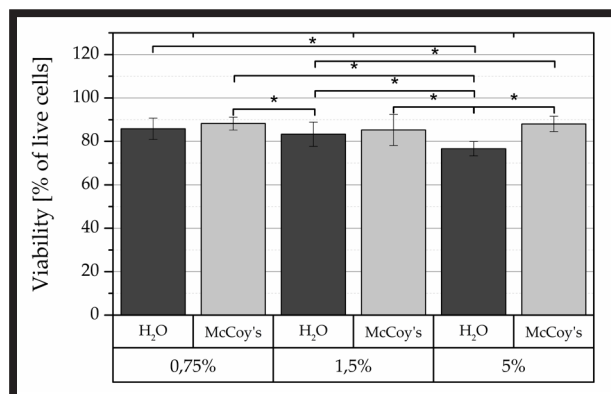


FIG. 4. Evaluation results of the degree of the Saos-2 line cell survival rate depending on the cross-linking solution concentration of the CaCl_2 -based hydrogel and the type of solvent used for its preparation (H_2O , culture medium McCoy's).

The analysis performed in the scope of the present study showed that the application of a cross-linking solution based on CaCl_2 of McCoy's 5A culture medium as a solvent, analogous to the solvent used to prepare the polymer composition, leads to an increase in the viability of the cells incorporated into cross-linked hydrogels. This phenomenon may result from an interaction of calcium ions with components contained in the culture medium.

With the purpose of obtaining hydrogel structures with a higher degree of cross-linking, potentially greater stability, and better strength properties, with simultaneous preservation of a high cell survival rate, for further testing, the cross-linking solution with the concentration of 5% prepared in McCoy's 5A culture medium was used.

The results of the live/dead assay given in FIG. 5, presenting images of the cells incorporated inside the cross-linked hydrogel bioinks, prove that the biological material was uniformly distributed in the whole volume of the hydrogel. In each of the samples, the cells adapt the spherical morphology for all the analyzed variants of cross-linking solutions, which is commonly observed for the biological material contained inside sodium alginate-based hydrogels [23].

Optimization results of the combining method of alginate-gelatin solutions with the cell pellet

The results of the analysis of the effect of the combination method of hydrogel materials with Saos-2 line cell pellet are shown in FIG. 6. The study showed that the highest survival rate of osteoblast cells, equal to $90.9 \pm 1.6\%$, was observed in the samples in which cells before combining with hydrogel were suspended in an 8% volume of culture medium used to prepare the hydrogel and slightly lower in those suspended in 2% volume of culture medium used to prepare the hydrogel. The lowest survival rate was observed in the samples in which the cell pellet was directly combined with the hydrogel material - in this case, the cell viability was $71.1 \pm 1.5\%$. The results obtained showed that the amount of the culture medium used to prepare the cell suspension before its combination with the polymer solution has a crucial role in ensuring the high survival rate of the cells incorporated into the bioink. With the increasing volume of the culture medium used for suspension of the cell pellet, the viability of the cells in the produced hydrogel structures increases. This phenomenon may be caused by a reduction of the shearing forces acting on the biological material previously placed in the cell suspension during the process of its combination with the hydrogel compared to the direct mixing of the cell pellet with the polymer solution.

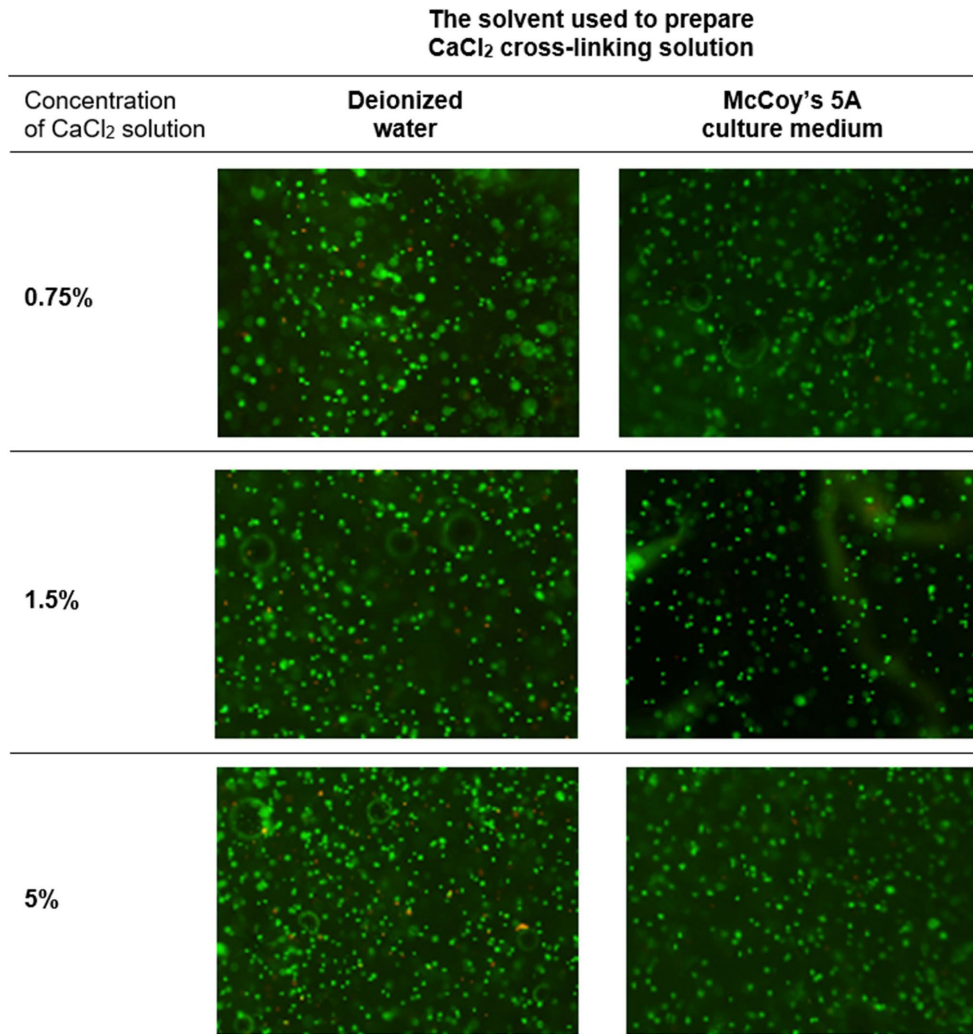
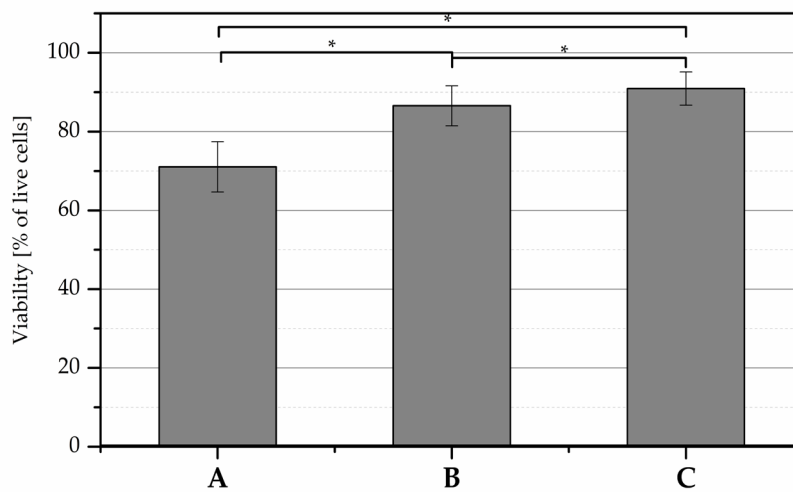


FIG. 5. Examples of the images obtained in the live/dead survival rate assessment of the Saos-2 line cells for the samples after cross-linking with different CaCl₂ solutions.



- A - direct connection of the hydrogel with the cell pellet by pipetting
 B - a combination of cell pellet with 2% of the volume of the culture medium used to prepare the hydrogel
 C - a combination of cell pellet with 8% of the volume of the culture medium used to prepare the hydrogel

FIG. 6. Evaluation results of the Saos-2 line cells survival rate depending on the combining method of the biological material with the hydrogel.

Results of evaluation of rheological properties of the polymer solution containing 2%Alg 9%Gel (w/v) used for 3D printing process

The curve of viscosity dependence as a function of shear rate, presented in FIG. 7, developed for a polymer solution containing 2%Alg 9%Gel (w/v) prepared in a method optimized during the experiments described in the previous sections, indicates that the viscosity of the developed polymer solution changes as a function of the shear rate. The obtained dependence proves that the material is a non-Newtonian fluid. With increasing shear rate, the viscosity of the polymer solution decreases in the range from the initial maximum values of 5.2551 Pa·s to 0.4786 Pa·s. The course of the curve proves the ability of the material to shear thinning. This is a very important characteristic of the polymer solution during 3D bioprinting processes, which makes it possible to reduce the force needed to extrude the material and decrease the shear stress during the printing process. The use of too high shear stresses related to the extrusion of the bioink can cause mechanical damage of the biological material contained in the printed structures [28,29].

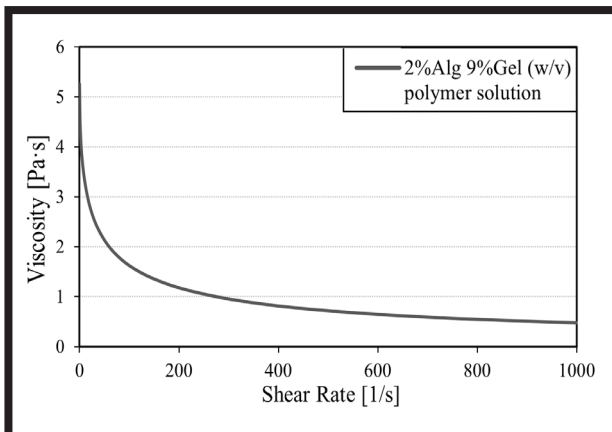


FIG. 7. Viscosity curve for a polymer solution containing 2%Alg 9%Gel (w/v) prepared in a method optimized during previous experiments that ensures the highest viability of the biological material before the 3D bioprinting process.

Evaluation results of the effect of the waiting time of the bioink for 3D printing and the effect of the 3D bioprinting process itself on the viability of the cells contained in the hydrogel printouts

The results of the analysis of the effect of the 3D direct printing process on the survival rate of the cells contained in the bioink are presented in FIG. 8. The study showed that the 3D bioprinting process does not reduce the cell survival rate. Available literature data have also confirmed the non-destructive character of 3D printing toward biological material [20]. For each of the hydrogel bioink variants tested, the viability of the Saos-2 line cells in final printouts is higher than 97%. The results of the live/dead assay (FIG. 9) prove that the biological material was uniformly distributed throughout the volume of the manufactured structure. The 3D bioprinting process allowed to obtain a higher survival rate of the biological material than in the case of the above-described studies leading to the production of the samples without using 3D printing. This phenomenon can be the result of the production of the structures with a layer thickness of about 250 μm during the 3D printing, which was not possible in the case of the samples poured on the surface of test plates. The high thickness of the samples can significantly limit the access of nutrients and gas exchange to the biological material incorporated inside the gel, which may result in a reduction in its viability [30].

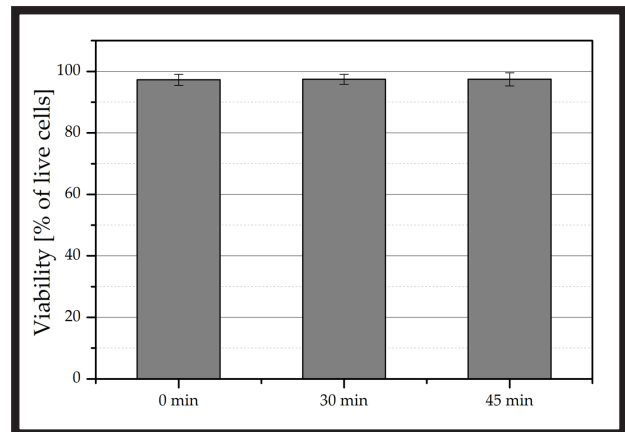


FIG. 8. Evaluation results of the degree of the survival rate of the Saos-2 line cells contained in the hydrogel printouts as a function of the waiting time of the bioink for the 3D printing process.

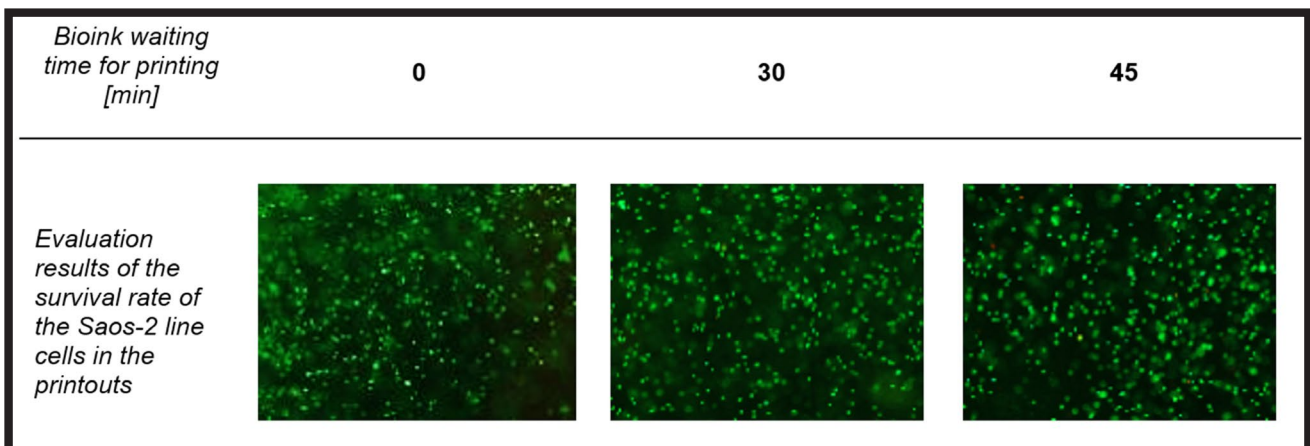


FIG. 9. Examples of the images obtained in the live/dead survival rate assessment of the Saos-2 line cells in the hydrogel printouts in relation to the bioink waiting time used for the 3D bioprinting process.

The analysis also demonstrated that the waiting time of the hydrogel bioink for 3D printing, prolonged even up to 45 min, does not reduce the cell survival rate in the final printouts. This observation provides an important aspect of the printouts preparation process. Using the manufacturing parameters mentioned earlier, the 45-minute time is sufficient for printing the structures with the entire volume of the hydrogel bioink placed in a syringe with a capacity of 5 ml typically applied in bioinks extrusion. One of the key parameters responsible for achieving high cell viability in the printouts is the incubation temperature of the prepared hydrogel bioink. The results of the study conducted by the team of L. Ouyang and collaborators indicate that an extended 3D bioprinting process at temperatures below 30°C for up to 40 min results in a significant decrease in the viability of cells in the obtained structures [31]. This phenomenon is a result of the gelatin sol-gel transition, which is the thermal crosslinking at a temperature of approximately 20-30°C. Literature data indicate that the melting point of gelatin-based hydrogels is about 28°C [19]. The use of a lower temperature during the 3D bioprinting process results in the necessity to increase the shear forces applied to the biological material during bioink extrusion. The results obtained during our experiment prove that a decrease in cell viability inside the hydrogel bioink after its incubation for 45 min at 37°C is not observed because the prepared hydrogel bioink did not undergo a process of thermal cross-linking of gelatin. Previous studies conducted by members of our team prove that with increasing temperature, the viscosity of the tested hydrogel is lower [32]. The 3D bioprinting process carried out in the current experiment was conducted at a temperature above the crosslinking of gelatin, which did not generate the need to increase the pressure during extrusion, and consequently to apply higher shear forces acting destructively on the biological material in the printouts.

Evaluation results of the effect of incubation time of 3D printouts on the viability of the cells contained in them

The analysis of the changes in the viability of the Saos-2 line cells contained in the hydrogel printouts after individual periods of their incubation in McCoy's 5A culture medium presented in FIGs. 10 and 11 demonstrate that together with the increasing incubation time of the printouts, cell survival rate decreases. However, in all the cases, it was higher than 70%. Directly after the 3D bioprinting process, the viability of the cells in the hydrogel printouts was nearly 97%.

After 24 hours of the printouts incubation, the cell viability was equal to $93.0 \pm 2.0\%$, whereby after three days, the viability was $84.0 \pm 0.6\%$ compared to the cell viability of the samples that were not subjected to the degradation process. The decrease in the viability of the cells incorporated into printouts recorded during the study may result from the release of calcium ions cross-linking the hydrogel. Sodium alginate-based hydrogels cross-linked with calcium ions in physiological conditions undergo reactions of the exchange of divalent Ca^{2+} ions to monovalent Na^+ ions present in the degradation medium [21]. This process leads to a gradual de-cross-linking of the hydrogel. The literature data have shown that the release of calcium ions from the printouts occurring in high amounts during discussed processes may demonstrate a cytotoxic effect [33]. The cause of the reduction in cell viability may also be the process of gelatin release from the hydrogel structures. At temperatures above 25°C, gelatin starts to form a liquid, which dissociates at a temperature of incubation of 37°C. Under such conditions, the gelatin not bound to the cross-linked blocks of alginate undergoes liquefaction, which in turn leads to its gradual washing out from the material [20,33]. Gelatin has RGD peptide sequences in its structure, promoting adhesion, migration, and differentiation of the cells.

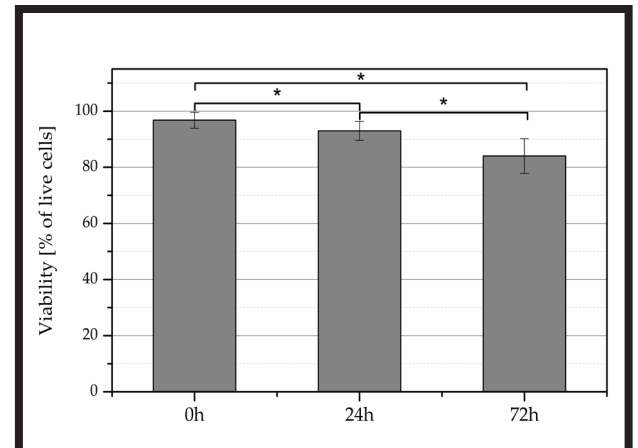


FIG. 10. Evaluation results of the degree of the Saos-2 line cells survival rate contained in the hydrogel printouts right after manufacturing (0 h) and after 24 h and 72 h incubation in standard conditions.

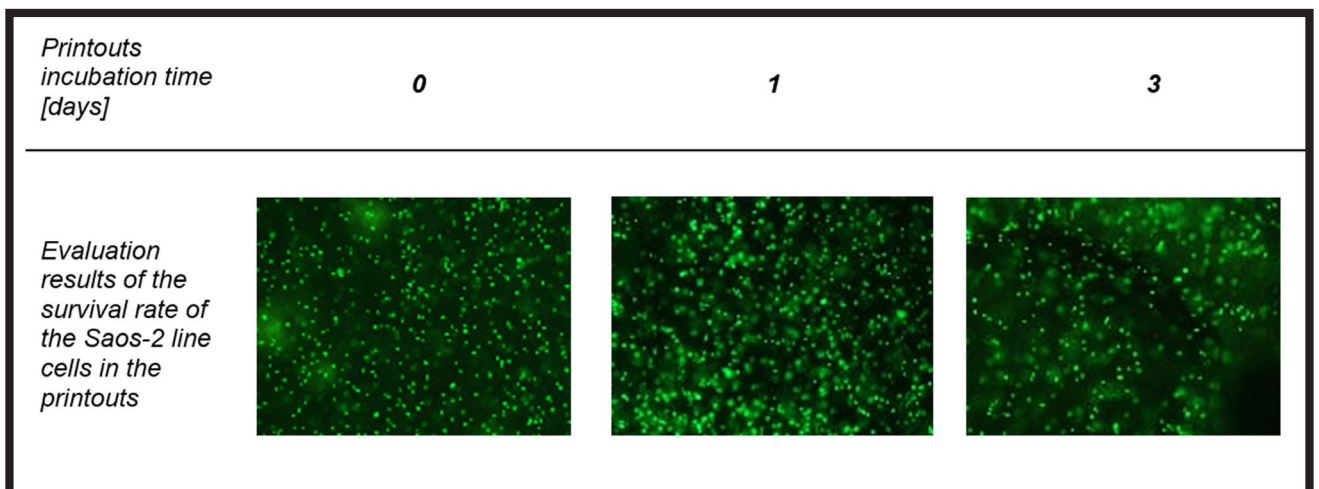


FIG. 11. Examples of the images obtained in the live/dead survival rate assessment of the Saos-2 line cells in the hydrogel printouts after individual incubation periods in standard conditions.

Therefore, as a result of the gelatin release, a reduction in the number of biological groups promoting the viability of the cells may occur. The survival rate of the cells contained in the hydrogel material may also undergo a reduction as an effect of the application of overly high concentrations of the polymer solutions forming a hydrogel. Higher concentrations of bioink components prevent cell migration and nutrient diffusion due to the entangled polymer network, which results in a high rigidity of the material [20]. In order to analyze the possibilities of improvement of the survival rate of the cells contained in the printouts during incubation processes, it is necessary to perform further research. It should focus on a material composition characterized by reduced structure rigidity with a lower content of the alginate, of which the rheological properties will enable the 3D bioprinting process. It is also essential to try to reduce the thickness of the hydrogel print path with the aim to ensure higher permeability of the structure for the nutrients contained in the culture medium, metabolic product removal, and enhance the efficiency of gas exchange [28,34].

Conclusions

The research conducted within the framework of this study proves that the 3D bioprinting process itself does not affect the cell survival rate. One of the factors determining the survival rate of the biological material at the stage of the hydrogel bioink preparation is the method of combining the biological material with the polymer solution. The analysis demonstrated that the preparation of the cell pellet suspension in the largest possible volume of the culture medium directly before the mixing procedure with hydrogel solution, provides the highest viability of the cells in the bioink. The obtained results also indicated that an important parameter determining the viability of the cells in the hydrogel printouts is the solvent used for the preparation of the CaCl_2 cross-linking solution. It was demonstrated that the preparation of the cross-linking solution based on the culture medium provides a higher survival rate of the cells in the hydrogel printouts with respect to commonly used aqueous solutions. In addition, the performed tests confirmed that the prolonged 3D printing waiting time of the hydrogel bioink up to 45 min does not reduce the cell survival rate in the final manufactured structures.

The selection of the individual manufacturing process parameters of the alginate- and gelatin-based hydrogel bioinks, such as the combining method of the polymer solution with the biological material, concentration, and the solvent used to prepare the cross-linking solution based on CaCl_2 , and also the waiting time of the prepared hydrogel bioinks for the 3D bioprinting process have the critical impact on the survival rate of the biological material contained in the hydrogel printouts. The results of the experiments performed demonstrate that with the application of the most optimal process parameters of the hydrogel bioinks preparation directly after the 3D printing, the survival rate of the model Saos-2 line cells every time reaches values exceeding 96%. The observations of the changes in the survival rate of the osteoblast-like cells in the hydrogel printouts for individual periods of time indicate that with increasing incubation time of the samples, the survival rate of the cells undergoes a gradual reduction, which may be the result of the release of the gelatin and calcium ions from the hydrogel or potentially overly high rigidity of the material's structure.

Acknowledgements

This research was funded by the National Centre for Research and Development under grant no. TECHMAT-STRATEG2/407770/2/NCBR/2020.

This work was completed while the first author was a Doctoral Candidate in the Interdisciplinary Doctoral School at the Lodz University of Technology, Poland.

ORCID iD

A. Wierzbicka:  <https://orcid.org/0000-0002-2740-4406>
 M. Bartniak:  <https://orcid.org/0000-0001-6753-8866>
 K. Rosińska:  <https://orcid.org/0000-0001-7240-5160>
 D. Bociąga:  <https://orcid.org/0000-0001-6230-4219>

References

- [1] Pietryga K.: Hydrożele. in Błażewicz S., Marciniak J.: *Monografia Inżynieria Biomedyczna Podstawy i Zastosowania Tom 4. Biomateriały*, Akdemicka Oficyna Wydawnicza EXIT, Warszawa 2016, 404-416.
- [2] Bahram M., Mohseni N., Moghtader M.: An Introduction to Hydrogels and Some Recent Applications., in Majee S.B.: *Emerging Concepts in Analysis and Applications of Hydrogels*, IntechOpen (2016) 137-144.
- [3] Wichterle O., Lím D.: Hydrophilic gels for biological use. *Nature* 185 (1960) 117-118.
- [4] Kopeček J.: Hydrogels: From soft contact lenses and implants to self-assembled nanomaterials. *Journal of Polymer Science, Part A: Polymer Chemistry* 47 (2009) 5929-5946.
- [5] Aswathy S.H., Narendrakumar U., Manjubala I.: Commercial hydrogels for biomedical applications. *Heliyon* 6 (2020) e03719.
- [6] Ahmed E.M.: Hydrogel: Preparation, characterization, and applications: A review. *Journal of Advanced Research* 6 (2015) 105-121.
- [7] Łabowska M.B., Cierluk K., Jankowska A.M., Kulbacka J., Detyna J., Michalak I.: A review on the adaption of alginate-gelatin hydrogels for 3D cultures and bioprinting. *Materials* 14 (2021) 858.
- [8] Bian L.: Functional hydrogel bioink, a key challenge of 3D cellular bioprinting. *APL Bioengineering* 4 (2020) 3-6.
- [9] Unagolla J.M., Jayasuriya A.C.: Hydrogel-based 3D bioprinting: A comprehensive review on cell-laden hydrogels, bioink formulations, and future perspectives. *Applied Materials Today* 18 (2020) 100479.
- [10] Mandrycky C., Wang Z., Kim K., Kim D.H.: 3D bioprinting for engineering complex tissues. *Biotechnology Advances*, 34 (2016) 422-434.
- [11] Nelson C., Tuladhar S., Launen L., Habib A.: 3D bio-printability of hybrid pre-crosslinked hydrogels. *International Journal of Molecular Sciences* 22 (2021) 13481.
- [12] Pawar S.N., Edgar K.J.: Alginate derivatization: A review of chemistry, properties and applications. *Biomaterials* 33 (2012) 3279-3305.
- [13] Ahearne M.: Introduction to cell-hydrogel mechanosensing. *Interface Focus* 4 (2014) 20130038.
- [14] Neves M.I., Moroni L., Barrias C.C.: Modulating Alginate Hydrogels for Improved Biological Performance as Cellular 3D Microenvironments. *Frontiers in Bioengineering and Biotechnology* 8 (2020) 665.
- [15] Abasalizadeh F., Moghaddam S.V., Alizadeh E., Akbari E., Kashani E., Fazljou S., Torbati, M., Akbarzadeh A.: Alginate-based hydrogels as drug delivery vehicles in cancer treatment and their applications in wound dressing and 3D bioprinting. *Journal of Biological Engineering* 14:8 (2020).
- [16] Jia J., Richards D.J., Pollard S., Tan Y., Rodriguez J., Visconti R.P., Trusk T.C., Yost M. J., Yao H., Markwald R.R., Mei Y.: Engineering alginate as bioink for bioprinting. *Acta Biomaterialia* 10 (2014) 4323-4331.
- [17] Sarker B., Singh R., Silva R., Roether J.A., Kaschta J., Detsch R., Schubert D.W., Cicha I., Boccaccini A.R.: Evaluation of fibroblasts adhesion and proliferation on alginate-gelatin crosslinked hydrogel. *PLoS ONE* 9 (2014) e107952.
- [18] Panwar A., Tan L.P.: Current status of bioinks for micro-extrusion-based 3D bioprinting. *Molecules* 21 (2016) 685.
- [19] Wang X., Ao Q., Tian X., Fan J., Tong H., Hou W., Bai S.: Gelatin-based hydrogels for organ 3D bioprinting. *Polymers* 9 (2017) 401.
- [20] Zhang J., Wehrle E., Vetsch J.R., Paul G.R., Rubert M., Müller R.: Alginate dependent changes of physical properties in 3D bioprinted cell-laden porous scaffolds affect cell viability and cell morphology. *Biomedical Materials* 14 (2019) 065009.
- [21] Lee K.Y., Mooney D.J.: Alginate: Properties and biomedical applications. *Progress in Polymer Science* 37 (2012) 106-126.
- [22] European Committee for Standardization, International Standard ISO 10993-5:2009 Biological evaluation of medical devices - Part 5: Tests for in vitro cytotoxicity. *Polski Komitet Normalizacyjny*, 2009.
- [23] Cao N., Chen X.B., Schreyer D.J.: Influence of Calcium Ions on Cell Survival and Proliferation in the Context of an Alginate Hydrogel. *ISRN Chemical Engineering* (2012) 1-9.
- [24] GhavamiNejad A., Ashammakhi N., Wu X.Y., Khademhosseini A. Crosslinking Strategies for 3D Bioprinting of Polymeric Hydrogels. *Small* 16 (2020) e2002931.
- [25] Fischer L., Nosratlo M., Hast K., Karakaya E., Ströhlein N., Esser T.U., Gerum R., Richter S., Engel F., Detsch R., Fabry B., Thievsen I.: Calcium supplementation of bioinks reduces shear stress-induced cell damage during bioprinting. *Biofabrication* 14 (2022) 045005.
- [26] Lee K.Y., Rowley J.A., Eiselt P., Moy E. M., Bouhadir K.H., Mooney D.J.: Controlling Mechanical and Swelling Properties of Alginate Hydrogels Independently by Cross-Linker Type and Cross-Linking Density. *Macromolecules* 33 (2000) 4291-4294.
- [27] Dubbin K., Tabet A., Heilshorn S.C.: Quantitative criteria to benchmark new and existing bio-inks for cell compatibility. *Biofabrication* 9 (2017) 044102.
- [28] Chen Y., Xiong X., Liu X., Cui R., Wang C., Zhao G., Zhi W., Lu M., Duan K., Weng J., Qu S., Ge J.: 3D Bioprinting of shear-thinning hybrid bioinks with excellent bioactivity derived from gellan/alginate and thixotropic magnesium phosphate-based gels. *Journal of Materials Chemistry B*, 8 (2020) 5500-5514.
- [29] Li H., Tan Y.J., Leong K.F., Li L.: 3D Bioprinting of Highly Thixotropic Alginate/Methylcellulose Hydrogel with Strong Interface Bonding. *ACS Applied Materials & Interfaces*. 9 (2017) 20086-20097.
- [30] Koch F., Tröndle K., Finkenzeller G., Zengerle R., Zimmermann S., Koltay P.: Generic method of printing window adjustment for extrusion-based 3D-bioprinting to maintain high viability of mesenchymal stem cells in an alginate-gelatin hydrogel. *Bioprinting* (2020) e00094.
- [31] Ouyang L., Yao R., Zhao Y., Sun W.: Effect of bioink properties on printability and cell viability for 3D bioplotting of embryonic stem cells. *Biofabrication* 8 (2016) 035020.
- [32] Bociaga D., Bartniak M., Grabarczyk J., Przybyszewska K.: Sodium Alginate/Gelatine Hydrogels for Direct Bioprinting - The Effect of Composition Selection and Applied Solvents on the Bioink Properties. *Materials* 12 (2019) 2669.
- [33] Giuseppe M.D., Law N., Webb B., A Macrae R., Liew L.J., Sercombe T.B., Dillely R. J., Doyle B.J.: Mechanical behaviour of alginate-gelatin hydrogels for 3D bioprinting. *Journal of the Mechanical Behavior of Biomedical Materials* 79 (2018) 150-157.
- [34] Zhang B., Gao L., Gu L., Yang H, Luo Y., Ma L.: High-resolution 3D Bioprinting System for Fabricating Cell-laden Hydrogel Scaffolds with High Cellular Activities. *Procedia CIRP* 65 (2017) 219-224.

BIOLOGICAL AND MECHANICAL RESEARCH OF TITANIUM IMPLANTS COVERED WITH BACTERICIDAL COATING

KLAUDIA MALISZ , BEATA ŚWIECZKO-ŻUREK* 

INSTITUTE OF MACHINES AND MATERIALS TECHNOLOGY,
FACULTY OF MECHANICAL ENGINEERING
AND SHIP TECHNOLOGY,
GDAŃSK UNIVERSITY OF TECHNOLOGY,
11/12 NARUTOWICZA STR., 80-233 GDAŃSK, POLAND
*E-MAIL: BEATA.SWIECZKO-ZUREK@PG.EDU.PL

Abstract

Materials used in bone implants should not only be non-toxic to the surrounding tissues, but also should promote osseointegration and minimize the risk of infection. Infections are a serious problem contributing to implantation failure. They are associated with pain, immobilization, and the necessity of reoperation. In extreme cases, they can lead to significant inflammatory changes in the bones, which, in turn, can lead to amputation and even death. After implantation, the surrounding tissues are damaged. In addition, implants are susceptible to bacterial colonization due to the lack of microcirculation. Therefore, scientists are working on antibacterial coatings to prevent the adhesion of bacteria before tissue regeneration.

The paper concerns the biological and mechanical properties of titanium implants with an antibacterial coating. The Ti13Zr13Nb alloy samples were coated with hydroxyapatite (HAp) coatings using the electrophoretic deposition technique (EPD). Subsequently, the surface of the samples was modified with silver, copper, and nickel nanoparticles by the immersion method. Different titanium sample types (i.e. HAp-only and nanometals-enriched coatings) were placed in a bacterial solution for a period of one month. Each sample was examined using scanning electron microscopy (SEM), nanoindentation, nanoscratch, and contact angle tests. The significant amount of dead biofilm on the surface proves the effectiveness of antibacterial activity. The wettability assessment showed that the samples were hydrophilic. The conducted tests of mechanical properties indicate the heterogeneity of the coatings.

Keywords: nanometals, scanning electron microscopy, wettability, nanoindentation, antibacterial properties, mechanical properties

[Engineering of Biomaterials 165 (2022) 17-22]

doi:10.34821/eng.biomat.165.2022.17-22

Submitted: 2022-10-09, Accepted: 2022-12-07, Published: 2022-12-08



Copyright © 2022 by the authors. Some rights reserved.
Except otherwise noted, this work is licensed under
<https://creativecommons.org/licenses/by/4.0>

Introduction

Infections are a serious problem that contributes to implant failure. They are associated with pain, immobilization, and also with repeated surgery. In extreme cases, they can lead to significant bone inflammation, which, in turn, may result in amputation or even death. Sources of infectious bacteria include the environment of the operating room, surgical equipment, clothing worn by the medical and paramedical staff, resident bacteria on the patient's skin and bacteria already residing in the patient's body [1].

Implants are particularly susceptible to bacterial colonization due to damage to the microcirculation. Microcirculation plays an important role in the immune system's defence response and antibiotics delivery. Therefore, if bacterial adhesion occurs before tissue regeneration, the host's immune system is often unable to prevent the colonization of microorganisms producing a biofilm matrix. The inhibition of microbial adhesion is essential to prevent postoperative infections [1].

Numerous implant-related infections are caused by staphylococci (roughly four out of five), and two single staphylococcal species, i.e. *Staphylococcus aureus* and *Staphylococcus epidermidis*, account for two out of three infection isolates. They represent, in absolute, the main causative agents in orthopaedics [1].

Biofilms are bacterial communities growing together embedded in an extracellular matrix which is a fundamental structural component of the bacterial community and acts as a protective shield [2]. Microorganisms contained in a biofilm can demonstrate up to 1000 times greater resistance to antibiotics compared to organisms of the same species in the form of plankton. In addition, a biofilm has significantly greater resistance to disinfectants ensured by a complex, cross-linked, hydrophobic structure with reduced gas permeability. The biofilm mode of growth of infecting bacteria on an implant surface protects the organisms from the host immune system and antibiotic therapy [1-3].

Titanium and its alloys belong to the most developed metallic biomaterials used for long-term orthopaedic and dental implants. Among more than 40 alloys investigated so far, the Ti13Zr13Nb alloy has the most suitable mechanical properties, as compared to the most popular technical titanium alloys, Ti-6Al-4V and Ti-6Al-7Nb. The advantages of the Ti13Zr13Nb alloy include also the absence of potentially dangerous elements, such as Al and V, which are presumed to develop Alzheimer's disease and tissue disturbance [4]. The Ti6Al4V and Ti13Nb13Zr alloys have the elasticity modulus (114 GPa and 81.6 GPa, respectively [5]) most similar (from among metal biomaterials) to that of a human bone (18-19 GPa [6]). Moreover, additional modifications of the surface of titanium alloys enable appropriate osseointegration [7].

Bioceramics are the ceramic materials used to replace or regenerate damaged bone and muscular tissues in the human skeletal system. One of the most widely used bioceramics is calcium hydroxyapatite, due to its biocompatibility and mechanical properties close to that of a human bone [8]. Hydroxyapatite materials are of great interest to scientists. Due to their excellent biocompatibility, osteoconductive properties and similarity to the inorganic component of human bone, they are widely used as biomedical materials, e.g. as bone fillers, scaffolds in tissue engineering, bioactive coatings, drug, protein, and gene delivery systems [9].

Being a calcium-based ceramic compound, hydroxyapatite exhibits brittleness, a very high compressive strength (up to 917 MPa), and a very low tensile property. Young's modulus and Poisson's ratio of sintered HAp are directly proportional to its density (porosity). If density increases by 100%, Young's modulus can reach 117 GPa and fracture toughness can reach 1 MPa/m² [8]. Hydroxyapatite coatings can be deposited on titanium substrates using many techniques. The most popular technique is electrophoretic deposition, in which whole HAp particles dispersed in organic alcohol achieve the electric charge, allowing them to deposit on an electrode as a very thin layer [4]. Other methods involve precipitation, the sol-gel method, and the hydrothermal method. Hydroxyapatite has also antibacterial properties, affecting both gram-negative bacteria and gram-positive bacteria thanks to its ability to penetrate the bacterial cell wall through electrostatic action. Hydroxyapatite nanoparticles (nanoHAp) have a wide spectrum of antibacterial activity and can potentially be used in medicine and environmental protection [10]. HAp is used in bone tissue engineering alone or can be doped with various metallic or non-metallic dopants to tailor its properties. Substitution enhances the properties of modified HAp depending on the properties of a dopant [8]. Despite numerous advantages, a noticeable disadvantage of bioceramic coatings (e.g. HAp, nanoHAp) deposited on metallic implants is their tendency to crack and poor adhesion to the substrate. Modifications of the chemical composition of applied coatings can be considered one of the possibilities to alleviate this problem [11].

To ensure the best properties of the material, scientists modify the surface of implants, often using materials in nanometric scale. The use of nanomaterials and nanostructures has revolutionized many fields of medicine and has led to a significant expansion of the list of implantable biomaterials and medical devices. Nanometals are often used due to their unique properties, including antimicrobial and anti-inflammatory ones [12]. Postoperative treatment following implantation is carried out by administering antibiotics. Similar effects can be achieved by the addition of some nanometals, operating as biocidal agents, to the coating.

Silver is usually applied directly to the implant surface as a pure metal or nanosilver [13]. Geissel et al. proved the antibacterial properties of silver nanoparticles using a scanning electron microscope. They showed that *Staphylococcus aureus* bacteria grown on pure SiO₂ had an intact and globally shaped shell, while the samples enriched with silver revealed a damaged cell structure of the surface of the bacteria attached to the particles [14].

The emerging problem of multi-drug resistance and its consequences stimulate researchers to search for effective alternatives to fight biofilm formation. Although the antibacterial properties of materials such as silver, nickel, and copper have been confirmed, it is recommended to create synergistic composite materials as bacterial pathogens can effectively develop resistance against metal nanophases. Therefore, it is very important to improve and maintain their antibacterial potential [15].

Despite the significant advantages of such approach, there is still a danger of negative effects on the human body. In an *in vitro* toxicity study of silver nanoparticles, even low exposure to silver nanoparticles induced oxidative stress and impaired mitochondrial functions. *In vivo* studies in rats on oral toxicity of nanosilver showed that nanosilver accumulated in the liver [16].

Copper is known not only for its high electrical and thermal conductivity but also for its antimicrobial properties. It has long been used as an effective antibacterial, antiviral, and antifungal agent. Copper nanoparticles are of interest for their excellent chemical, physical and optical properties, heat transfer, large surface area to volume ratio, as well as catalytic, magnetic, and biological properties [17-19].

Studies of antimicrobial activity have shown that copper oxide nanoparticles are effective as antimicrobial agents for both gram-positive and gram-negative bacteria. Bacteria have cell membranes with nanometer-sized pores which facilitate the penetration of nanoparticles. This is the cause of cytoplasm degradation, which ultimately leads to cell death. The antimicrobial mechanism is mainly attributed to the strong adsorption of ions to bacterial cells, which confers antimicrobial efficacy in a concentration-dependent manner [20].

Argueta-Figueroa et al. [20] synthesized nanoparticles of copper, nickel, and bimetallic Cu-Ni using a chemical method. Their antibacterial activity has been tested against the commonly used standard human pathogens *Staphylococcus aureus* (gram negative), *Escherichia coli* (gram positive), and additionally *Streptococcus mutans*. *Streptococcus mutans* is physiologically present in the human mouth and contributes to tooth decay. Studies have shown that copper nanoparticles exhibit bactericidal activity against *S. aureus*, *E. coli*, and *S. mutans*, while nickel nanoparticles and bimetallic Cu-Ni nanoparticles only exhibit bacteriostatic activity against the same microorganisms [20].

The paper deals with the analysis of hydroxyapatite (HAp) coatings (without additives and with nanometals) on the titanium alloy. The aim of the study is to compare the biological and mechanical properties of the samples.

Materials and Methods

Preparation of samples

The Ti13Zr13Nb alloy was used as a substrate. The surface was prepared by using abrasive paper SiC up to grit # 2500. The samples were then rinsed with isopropanol and ultrasonically cleaned.

Electrophoretic deposition of HAp coatings

The Ti13Zr13Nb alloy samples were covered with hydroxyapatite coatings by the electrophoretic technique. The EPD was carried out in a suspension prepared by dispersing 0.1143 g of HAp powder (Sigma-Aldrich) in 100 ml of ethanol (anhydrous, 99.8% purity). The EPD was performed at 8 V for 10 min at room temperature. The hydroxyapatite solution was mixed with a magnetic stir bar for 4-5 min prior to each sample procedure. Finally, the deposited coatings were air dried at room temperature for 24 h. Subsequently, the samples were sintered in a vacuum oven for 2 h at 500°C.

Immersion method

The surface of the samples was modified with silver, copper, and nickel nanoparticles using the immersion method. 0.005 g of nanoparticles were dispersed in 50 ml of 99.8% anhydrous alcohol. The size of the nanoparticles is shown in TABLE 1.

TABLE 1. Size of nanoparticles.

Nanoparticles	Size [nm]
Ag	40
Cu	10-30
Ni	10-30

Initiation of bacterial growth

All samples were immersed in a bacterial solution [21] for 30 days. The chemical composition of the solution is presented in TABLE 2, and the list of the added microorganisms in TABLE 3.

TABLE 2. Chemical composition of the bacterial solution [21].

Component	Content [g/dm ³]
Casein peptone	17
Pepton S	3
NaCl	5
Na ₂ HPO ₄	2.5
Glucose	2.5

TABLE 3. List of bacteria added to the solution [21].

Bacteria	Content in liquid [%]
Staphylococcus aureus	20
Staphylococcus epidermidis	20
Enterococcus faecalis	15
Enterobacter cloacae	10
Pseudomonas aeruginosa	35

Surface examination

The morphology of the samples was investigated by a Schottky field emission scanning electron microscope (FEI Quanta FEG 250) with an ET secondary electron detector. The beam accelerating voltage was kept at 10 kV. For the purpose of elemental analysis, energy dispersive X-ray spectroscopy was performed with the EDAX Genesis APEX 2i with the ApolloX SDD spectrometer.

Measurements of contact angle

Eight samples of titanium alloy with a hydroxyapatite coating were tested with the Attension Thete Lite goniometer to assess the wettability of the materials. A drop of water was dropped onto the sample surface. The computer program calculated the contact angle (CA) from the shape of the drop of water immediately after its contact with the surface of the sample, then the measurement was after 5 s and 10 s. The surface of the material is considered hydrophilic if the measured value is below 90° and hydrophobic above 90°.

Mechanical studies - nanoindentation and nanoscratch tests

Nanoindentation tests were performed using the NanoTest™ Vantage device. A Berkovich diamond indenter with an apex angle of 124.4° was used for the analysis. The parameters of the nanoindentation tests are shown in TABLE 4.

TABLE 4. The parameters of the nanoindentation tests.

Parameter	Value
Number of measurements	15
Maximum force [mN]	10
Loading time [s]	10
The dwell period at maximum load [s]	5
Unloading time [s]	10

The modulus of elasticity was calculated after transforming the formula [7]:

$$\frac{1}{E_r} = \frac{1 - \nu_s^2}{E_s} + \frac{1 - \nu_i^2}{E_i} \quad (1)$$

where ν_i is the nanoindenter Poisson's ratio (accepted as 0.07) [7], ν_s is the Poisson's ratio of the tested materials (accepted for HAp as 0.3 [4] and 0.27 for titanium alloy [7]), E_s is the elastic modulus of the tested samples, E_i is the Young's modulus of the nanoindenter (accepted as 1140 GPa) and E_r is the reduced modulus of elasticity [7]. The final equation from which the reduced Young's modulus was determined is:

$$E_s = \frac{E_i E_r (1 - \nu_s^2)}{E_i - E_r (1 - \nu_i^2)} \quad (2)$$

Nano-scratch tests were performed with the NanoTest™ Vantage (Micro Materials). The scratch tests were carried out by increasing the load from 0 mN to 200 mN at a loading rate of 1.3 mN/s at a distance of 500 μm. The adhesion of the coating was assessed based on the observation of an abrupt change in frictional force during the test.

Results and Discussions

Surface examination using a scanning electron microscope

Samples of Ti13Zr13Nb titanium alloy coated with hydroxyapatite with metal nanoparticles were examined using a scanning electron microscope. The received images are shown in FIG. 1.

The scanning electron microscope study showed numerous nanoparticles on the surface. The distribution of the nanoparticles was heterogeneous in the case of Ag and Cu. They also formed numerous agglomerates. The sample with nickel nanoparticles was characterized by the highest homogeneity of the nanoparticles distribution.

The SEM indicated changes in the topography of the implant surface with visible singular bacteria and biofilm colonies. The biofilm showed a tendency to capsulate the nanoparticles, but the cell structure of the bacteria on the surface of the nanoparticles was damaged. This phenomenon was also observed in the studies of the antibacterial properties of silver nanoparticles on SiO₂. Geissel et al. [14] detected that samples enriched with silver showed a damaged cell structure of the *Staphylococcus aureus* bacteria attached to the surface of the particles. The significant dead biofilm proved the antibacterial properties of the coatings. Bartmański et al. [4] presented high magnification SEM images that demonstrate the porous structure of the nanoHAp coatings. For nanoHAp coatings obtained at 0.1 g nanoHAp powder in the solution, the coatings roughness decreased with the increasing voltage, due to the presence of a smaller number of agglomerates on the surface.

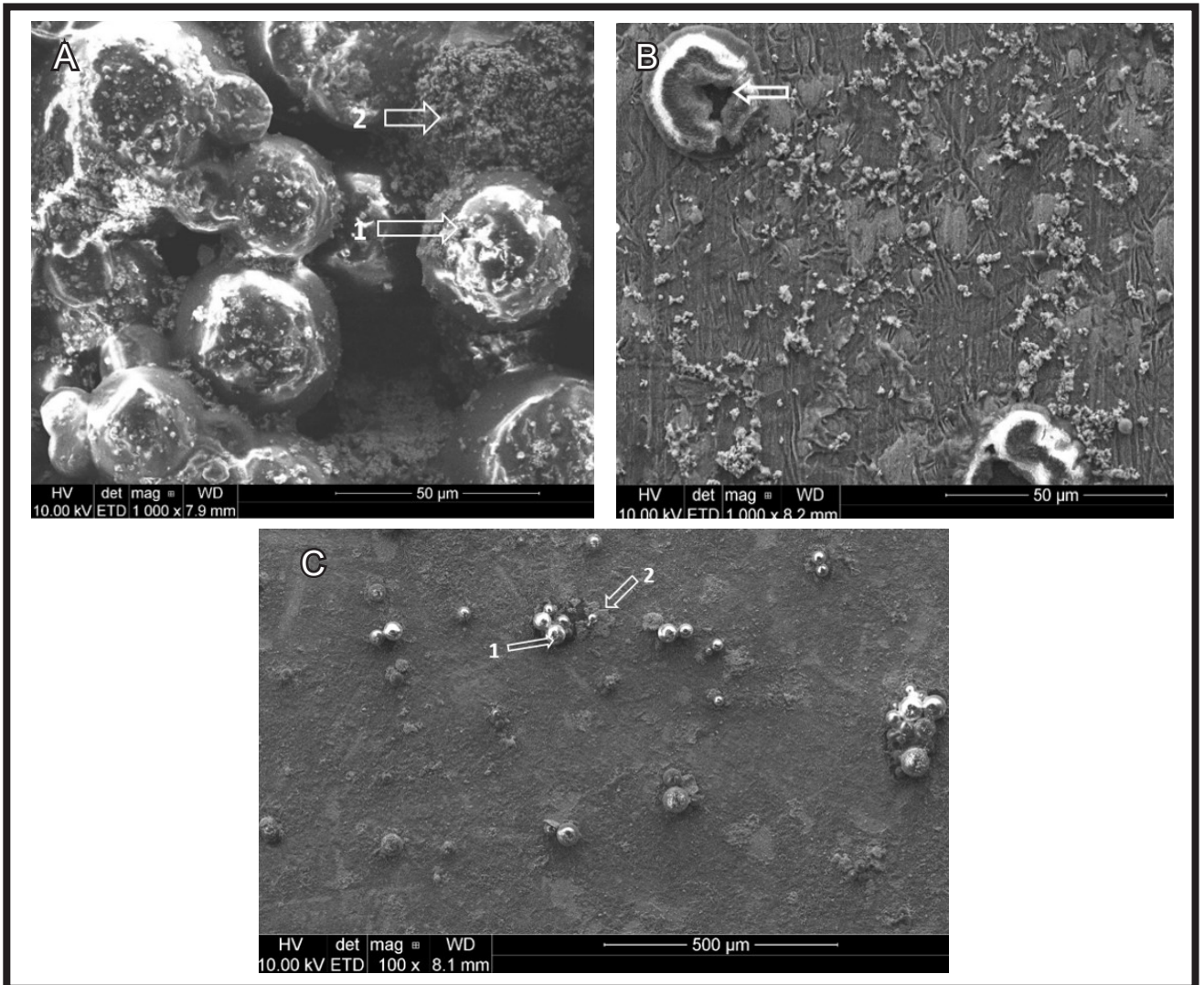


FIG. 1. Surfaces of the HAp coatings with the nanoparticles after 1 month in the bacterial solution. A) Image of the surface of titanium alloy with deposited HAp and silver nanoparticles, visible agglomerates of silver nanoparticles and a living (1) and dead biofilm (2). B) Surface image of titanium alloy with deposited HAp and nickel nanoparticles - visible Ni nanoparticles. C) Surface image of titanium alloy with deposited HAp and copper nanoparticles with visible nanoparticles (1) and dead biofilm (2).

Measurements of contact angle

TABLE 5 presents the results of the contact angles obtained for the tested materials; the results were averaged over 4 measurements. The volume of the drop of water was 4 μ l.

The wettability assessment showed that the samples were hydrophilic, which is consistent with the literature data. The lowest contact angle was observed for the sample with the additive-free hydroxyapatite coating (0°) and the highest contact angle occurred for the copper nanoparticles enriched implant (17.94°). The contact angle values of the hydroxyapatite samples with silver and nickel nanoparticles were 8.88° and 3.33° , respectively.

The nanoparticles significantly increase the value of the contact angle, which is consistent with the literature data [13]. Scientists concluded that the presence of silver nanoparticles on the surface may prevent water droplets from penetrating into the nanoHAp coating, resulting in an increase in the contact angle [13].

The low contact angle values for all specimens may be attributed to their porous surface structure. Contact angles are measures of wettability; their low values correspond to better osseointegration. On the other hand, the best values of contact angle for cell attachment were assessed at 55° and for bone regeneration at 35° to 80° [13]; these values are higher than those obtained in the presented studies.

TABLE 5. Results of the obtained contact angles for the samples as a function of time.

Time [s]	CA mean for the sample without nanoparticles [$^\circ$]	CA mean for the sample with Ag nanoparticles [$^\circ$]	CA mean for the sample with Cu nanoparticles [$^\circ$]	CA mean for the sample with Ni nanoparticles [$^\circ$]
0	67.77 ± 32.98	40.42 ± 17.0	24.35 ± 24.56	38.26 ± 4.6
5	29.57 ± 33.46	12.96 ± 8.0	50.44 ± 24.40	13.62 ± 4.92
10	0 ± 0	8.88 ± 7.3	17.94 ± 22.82	3.33 ± 5.76

Mechanical studies - nanoindentation and nanoscratch tests

FIG. 2 shows one of the nanoindentation load-displacement curve for the examined materials. The nanoindentation tests were performed for all HAp coatings with nanometals and for the titanium samples only after grinding. The mechanical properties - hardness and Young's modulus - are shown in TABLE 6. 15 nanoindentation measurements were pursued.

The nanoscratch tests were performed for HAp coating with nanometals. 5 measurements were made for each sample. The obtained results are shown in TABLE 7 based on the diagram of the depth change depending on the distance. First, the distance at which the coating was delaminated was determined, then the appropriate normal force for the distance covered by the tool was determined. The graphs of changes in surface topography before and after the nanoscratch tests are presented in FIG. 3.

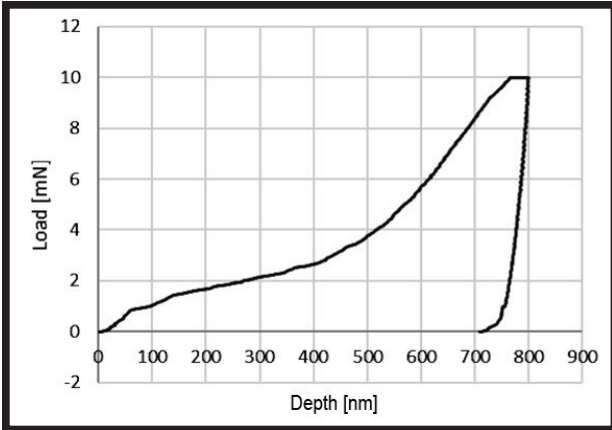


FIG. 2. Nanoindentation load-displacement curve obtained for HAp coating with Ni nanoparticles.

TABLE 6. Mechanical properties: hardness and Young's Modulus of samples.

Material	Hardness [GPa]	Young's modulus [GPa]
HAp with Ag nanoparticles	1.95 ± 1.10	74.88 ± 27.15
HAp with Cu nanoparticles	0.82 ± 0.34	55.13 ± 13.88
HAp with Ni nanoparticles	1.30 ± 1.10	80.66 ± 26.54

TABLE 7. Results of nanoscratch tests of the HAp coatings with nanometals.

Measurement	HAp with Ag nanoparticles		HAp with Cu nanoparticles		HAp with Ni nanoparticles	
	Distance [µm]	Load [mN]	Distance [µm]	Load [mN]	Distance [µm]	Load [mN]
1	64	25.6	13	5.2	47	18.8
2	86	34.4	39	15.6	108	43.2
3	82	32.8	68	27.2	100	40
4	80	32	75	30	100	40
5	80	32	68	27.2	119	47.6
average		31.36 ± 3.01		21.04 ± 9.35		37.92 ± 9.96

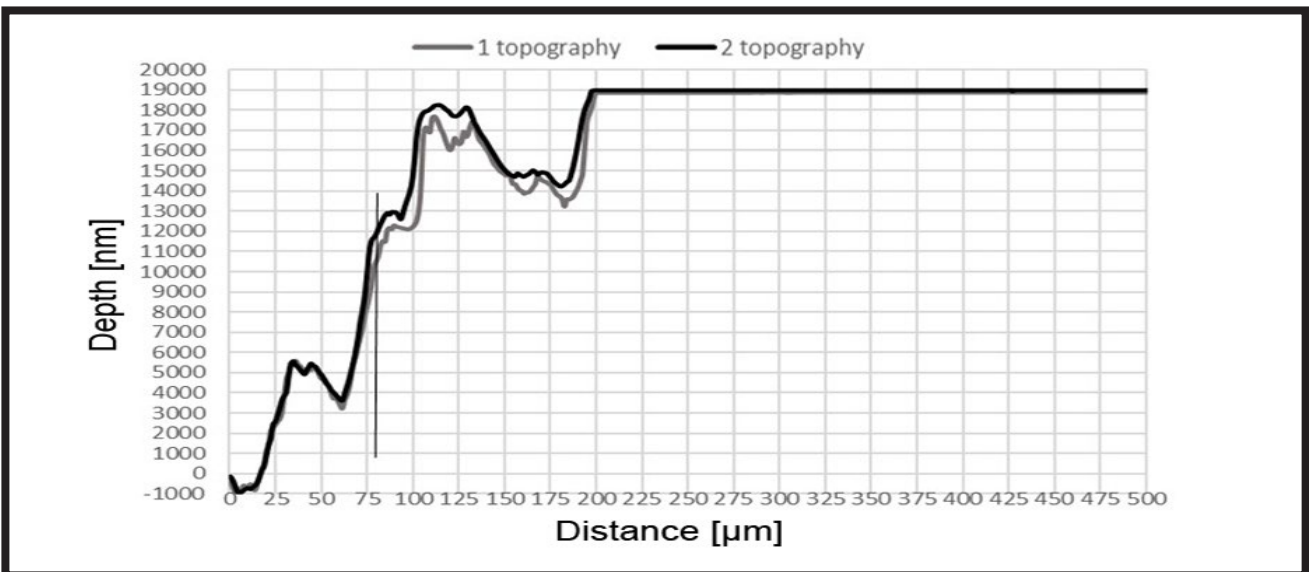


FIG. 3. Nanoscratch test of HAp coating with Ag nanoparticles. The delamination of the coating is marked in the graph (the black line).

The conducted tests of mechanical properties indicate the heterogeneity of the coatings due to the large standard deviation of the obtained hardness results, which is associated with high surface roughness. The greatest heterogeneity was revealed for the hydroxyapatite coating with nickel nanoparticles (1.30 ± 1.10 GPa), and the lowest for the hydroxyapatite coating with copper nanoparticles (0.82 ± 0.34 GPa). The coatings are characterized by low hardness; this value depends on the thickness of the coating (the greater the thickness, the harder the coating). The most advantageous Young's modulus was observed for the hydroxyapatite coating with copper nanoparticles (55.13 ± 13.88 GPa) and its value was the closest to the Young's modulus of bone. Young's modulus result was the highest for HAP with Ni nanoparticles and amounted to 80.66 ± 26.54 GPa. Bartmański et al. [11] observed that Ag nanoparticles addition had negligible influence on the coating's mechanical properties. Still, the presence of Cu nanoparticles, alone or with Ag nanoparticles, resulted in the increased value of hardness and Young's modulus. The positive impact of Cu nanoparticles may be attributed to somewhat decreasing porosity and susceptibility to brittle cracking.

The adhesion of coatings to the metallic substrate is one of the most essential properties determining the quality of the coatings. The loose particles in HAP coatings may even initiate inflammation process and disappearance of bone in its surroundings [4]. The sample with nickel nanoparticles had the best coating adhesion, where the force at which delamination occurred was 37.92 ± 9.96 mN. The smallest force causing delamination of the coating was observed for the sample with copper nanoparticles.

Conclusions

The Ti13Zr13Nb alloy samples were covered with hydroxyapatite coatings through the electrophoretic deposition. The samples surface was modified with silver, copper, and nickel nanoparticles. Eight titanium samples (i.e. an additive-free hydroxyapatite coating, a silver nanoparticles enriched implant, a copper nanoparticles enriched implant and a nickel nanoparticles enriched implant), were placed in a bacterial solution for a period of one month. Each sample was examined using a scanning electron microscope. Wettability and mechanical properties were also assessed.

The significant dead biofilm in their vicinity proves the effectiveness of antibacterial activity. All of the samples had visible high surface roughness, which was confirmed in nanohardness tests using the nanoindentation method. The coatings were characterized by a low hardness (this value depends on the thickness of the coating). The most advantageous Young's modulus was observed in the case of the hydroxyapatite coating with copper nanoparticles, as its value is most similar to the Young's modulus of bone. The sample with nickel nanoparticles had the best coating adhesion. All the samples were hydrophilic, which is associated with possible high osteointegration. In addition, the nanoparticles increased the contact angle value.

Acknowledgments

We thank Jakub Karczewski for help in taking pictures on a scanning microscope and Aleksandra Laska for help in carrying out the research. The research was financed by the Gdańsk University of Technology.

ORCID iD

K. Malisz:  <https://orcid.org/0000-0003-0596-3140>
B. Świeczko-Żurek:  <https://orcid.org/0000-0001-7742-0052>

References

- [1] Ribeiro M., Monteiro F. J., Ferraz M. P.: Infection of Orthopedic Implants with Emphasis on Bacterial Adhesion Process and Techniques Used in Studying Bacterial-Material Interactions. *Biomater* 2 (2012) 176-194.
- [2] Cendra M. del M., Torrents E.: Pseudomonas Aeruginosa Biofilms and Their Partners in Crime. *Biotechnol Adv* 49 (2021) 107734.
- [3] Vickery K.: Special Issue: Microbial Biofilms in Healthcare: Formation, Prevention and Treatment. *Materials* 12 (2019) 3-5.
- [4] Bartmański M., Zielinski A., Majkowska-Marzec B., Strugała G.: Effects of Solution Composition and Electrophoretic Deposition Voltage on Various Properties of Nanohydroxyapatite Coatings on the Ti13Zr13Nb Alloy. *Ceramics International* 44 (2018) 19236-19246.
- [5] Surma K., Adach M., Dębowska M., Turlej P.: Projektowanie i analiza obliczeniowa implantu krążka międzykręgowego odcinka szyjnego kręgosłupa przeznaczony do wytwarzania za pomocą technologii przyrostowych. *Aktualne problemy biomechaniki* 17 (2019) 111-122.
- [6] Świeczko-Żurek B.: *Biomateriały*; Wydawnictwo Politechniki Gdańskiej (2009) 72-97.
- [7] Jażdżewska M., Kwidzińska D., Seyda W., Frydrych D., Zielińska A.: Mechanical Properties and Residual Stress Measurements of Grade IV Titanium and Ti-6Al-4V and Ti-13Nb-13Zr Titanium Alloys after Laser Treatment. *Materials* 14 (2021) 1-22.
- [8] Panda S., Biswas C.K., Paul S.: A Comprehensive Review on the Preparation and Application of Calcium Hydroxyapatite: A Special Focus on Atomic Doping Methods for Bone Tissue Engineering. *Ceramics International* 47 (2021) 28122-28144.
- [9] Abdulkareem M.H., Abdalsalam A.H., Bohan A.J.: Influence of Chitosan on the Antibacterial Activity of Composite Coating (PEEK/HAP) Fabricated by Electrophoretic Deposition. *Progress in Organic Coatings* 130 (2019) 251-259.
- [10] Lin K., Chang J.: Structure and Properties of Hydroxyapatite for Biomedical Applications. In *Hydroxyapatite (Hap) for Biomedical Applications*; Woodhead Publishing (2015) 3-19.
- [11] Bartmański M., Pawłowski Ł., Mielewczyk-Gryń A., et al.: The Influence of Nanometals, Dispersed in the Electrophoretic Nanohydroxyapatite Coatings on the Ti13Zr13Nb Alloy, on Their Morphology and Mechanical Properties. *Materials* 14 (2021) 1-16.
- [12] Prasad K., Zhou R., Zhou R., Schuessler D., et al.: Cosmetic Reconstruction in Breast Cancer Patients: Opportunities for Nanocomposite Materials. *Acta Biomaterialia* 86 (2019) 41-65.
- [13] Bartmański M., Cieslik B., Glodowska J., et al.: Electrophoretic Deposition (EPD) of Nanohydroxyapatite - Nanosilver Coatings on Ti13Zr13Nb Alloy. *Ceramics International* 43 (2017) 11820-11829.
- [14] Geissel F. J., Platania V., Gogos A., et al.: Antibiofilm Activity of Nanosilver Coatings against Staphylococcus Aureus. *Journal of Colloid and Interface Science* 608 (2021) 3141-3150.
- [15] Vijayaraghavan P., Rathi M.A., Almaary K.S., et al.: Preparation and Antibacterial Application of Hydroxyapatite Doped Silver Nanoparticles Derived from Chicken Bone. *Journal of King Saud University - Science* 34 (2022) 101749.
- [16] Prabhu S., Poulouse E.K.: Silver Nanoparticles: Mechanism of Antimicrobial. *Int. Nano Lett.* 2 (2012) 32-41.
- [17] Ghuglot R., Titus W., Agnihotri A.S., Krishnakumar V., et al.: Stable Copper Nanoparticles as Potential Antibacterial Agent against Aquaculture Pathogens and Human Fibroblast Cell Viability. *Biocatalysis and Agricultural Biotechnology* 32 (2021) 101932.
- [18] Ingle A.P., Duran N., Rai M.: Bioactivity, Mechanism of Action, and Cytotoxicity of Copper-Based Nanoparticles: A Review. *Applied Microbiology and Biotechnology* 98 (2014) 1001-1009.
- [19] Ameh T., Sayes C. M.: The Potential Exposure and Hazards of Copper Nanoparticles: A Review. *Environmental Toxicology and Pharmacology* 71 (2019) 103220.
- [20] Argueta-Figueroa L., Morales-Luckie R.A., Scougall-Vilchis R.J., Olea-Mejia O.F.: Synthesis, Characterization and Antibacterial Activity of Copper, Nickel and Bimetallic Cu-Ni Nanoparticles for Potential Use in Dental Materials. *Progress in Natural Science: Materials International* 24 (2014) 321-328.
- [21] Świeczko-Żurek B.: Method of Assessing Biodegradation of Metallic Implants, Method of Obtaining a Bacterial Solution for Assessing Biodegradation of Metallic Implants and a Bacterial Composition for Assessing Biodegradation of Metallic Implants. Patent No. P 409082, 2015.

EXPERIMENTAL INVESTIGATIONS OF THE PMMA BONE CEMENT DISTRIBUTION INSIDE A MODEL OF LUMBAR VERTEBRAE

ARTUR BONIK^{1*}, ZBIGNIEW TYFA²,
LECHOSŁAW F. CIUPIK¹, KRZYSZTOF SOBCZAK²,
AGNIESZKA KIERZKOWSKA¹, DAMIAN OBIDOWSKI²,
DARIUSZ WITKOWSKI², TOMASZ PAŁCZYŃSKI²,
MARCIN ELGALAL³, PIOTR KOMOROWSKI³,
EDWARD SŁOŃSKI¹, KRZYSZTOF JÓZWIK²,
BOGDAN WALKOWIAK³

¹ LFC LTD. MEDICAL, 41 KOŻUCHOWSKA ST.,
65-364 ZIELONA GÓRA, POLAND

² LODZ UNIVERSITY OF TECHNOLOGY,
FACULTY OF MECHANICAL ENGINEERING,
INSTITUTE OF TURBOMACHINERY,
WÓLCZAŃSKA 219/223 ST., 90-924 ŁÓDŹ, POLAND

³ MOLECULAR AND NANOSTRUCTURAL BIOPHYSICS
LABORATORY, BIONANOPARK LABORATORIES,
114/116 DUBOIS ST., 93-465 LODZ, POLAND

*E-MAIL: ARTURBONIK@GMAIL.COM

Abstract

The use of bone cement in procedures such as vertebroplasty and kyphoplasty can reduce pain and mechanically support the spine. This study aimed to evaluate whether air entrapped within bone cement affected its distribution in a vertebral body model. The study included 3D printed anatomical models of vertebrae together with their internal trabecular structure. Aeration was achieved by mixing the bone cement using three different altered procedures, whilst the control sample was prepared according to the manufacturer's instructions. The further two samples were prepared by reducing or increasing the number of cycles required to mix the bone cement. A test rig was used to administer the prepared bone cement and introduce it into the vertebral model. Each time the injection was stopped when either the cement started to flow out of the vertebral model or when the entire cement volume was administered. The computer tomography (CT) scanning was performed to evaluate aeration and its influence on the bone cement distribution in each of the patient-specific models. The large number of small pores visible within the cement, especially in the cannula vicinity, indicated that the cement should not be treated as a homogenous liquid. These results suggest that a high level of aeration can influence the further cement distribution.

Keywords: percutaneous vertebroplasty, osteoporotic spinal fractures, spinal cement injection, cement distribution, bone cement preparation

[Engineering of Biomaterials 165 (2022) 23-30]

doi:10.34821/eng.biomat.165.2022.23-30

Submitted: 2022-12-18, Accepted: 2022-12-28, Published: 2022-12-30



Copyright © 2022 by the authors. Some rights reserved.
Except otherwise noted, this work is licensed under
<https://creativecommons.org/licenses/by/4.0>

Introduction

Osteoporosis causes a decrease in bone mass and a degeneration of the bone tissue microarchitecture in the spine section [1]. Compression and osteoporotic bone fractures are characteristic of osteoporosis [2]. Most compression and osteoporotic fractures are fixed within several months from the first complaint occurrence. During this period, conservative healing methods are used, such as massages, pharmacological treatments, and limiting movement [3]. In a situation where the pain caused by osteoporotic compression fractures [4] or vertebral body cancerous changes cannot be endured any longer, it is necessary to support the spine mechanically with vertebroplasty, kyphoplasty and/or by enhancing the spinal column with implants [5].

In mini-invasive enhancing procedures [6] such as vertebroplasty and kyphoplasty, the bone cement is injected with a needle into the damaged vertebrae under radiological supervision. Polymethylmethacrylate (PMMA) is used most frequently for this purpose [7]. A small amount of cement, ranging from 2.5 to 4.5 ml, is placed in the vertebrae, which is enough to restore its biomechanical parameters, as shown in numerous research results [8-9]. To avoid complications, the filling procedure is stopped when the cement approaches the defect, the anatomical orifice, or when the cement leaks out beyond the cortical bone of the vertebra in any direction [10].

Previous investigations [12] show that PMMA-based cement can be characterized by a variable level of aeration [13], which is strictly related to the cement mixing process. Aeration and compressibility can change the general material flow dynamics, especially the injection speed. The cement tenacity grows as a result of the components chemical reactions during the polymerization process, which increases the flow resistance.

The cement injection into the bone structure should be made during its optimal tenacity [14]. When the cement is applied at the too low tenacity, it can lead to uncontrollable liquefaction. If the cement tenacity is too high, the flow resistance can hinder its further propagation in the bone. As a result, not only will the intended outcome not be achieved [15], but the patient's health can be at serious risk [17]. The most common complication that occurs in the procedure is the cement leakage, defined as the bone cement escape beyond the vertebral body [16-18]. Most leaks are local and asymptomatic [19]. Otiz [20] divides complications related to the procedure of enhancing the vertebrae with bone cement into two groups. The first group covers local complications, consisting in damages and changes connected directly to the vertebrae surrounding. The second group is systemic complications which influence the systems and organs proper functioning. The majority of risks associated with transdermic vertebroplasty can be minimized by actions that prevent leaks, such as controlling the medium distribution.

The main objective of these investigations was to analyze via CT scans the influence of cement aeration on its distribution in the vertebral body model developed and 3D printed by the authors. During the last decade, PMMA-based cements and their features have been widely discussed. The research was mainly focused on creating new cements and composites, improving mechanical features [21], improving biological response [22], rheological and mechanical features of cement materials [23-27]. However, no research has been reported on the cement injection and its distribution in an anatomic model of vertebrae, built with the 3D printing technology. This indicates the novelty of the subject presented in this work. In order to achieve the intended purpose, experimental studies were carried out, requiring the preparation of suitable models and the use of several sets of biomedical cements.

Methodology

The conducted investigations composed of four phases. In the first phase, a digital reconstruction of the lumbar vertebra with osteoporotic changes was prepared by the computer microtomography based on anatomic medical data. The obtained model was segmented and processed digitally in order to be printed in the 3D technology. During the second phase, a precise physical model with an internal structure was printed with the 3D printer (Ultimaker 3, manufactured by Ultimaker B.V., The Netherlands). The next phase was to prepare the properly aerified bone cement and to inject it into the previously prepared models of vertebrae. The last phase consisted in an inspection of the bone cement distribution in the filled model with the computer microtomography.

Reconstruction

The anatomic digital data of the lumbar vertebra with osteoporotic changes, saved as a DICOM file (Digital Imaging and Communications in Medicine) were reconstructed and segmented with the Mimics Medical™ software developed by the Materialise company. Next, the data from the segmentation were subjected to digital processing. The model mesh was optimized with respect to the scope of the print, removing the too fine or loose elements. The back part was also removed, as it was irrelevant in the cement distribution analysis, leaving thus the vertebra alone. The model was modified by implementing a mechanical connection that ensured the same entry point into the vertebra and a repeatable injection point. The prepared 3D digital model was exported to a STL file, which allowed it to be imported and printed. FIG. 1 shows a view of the model with planes indicating its cross-sections, as well as the selected internal micro-architecture.

Physical 3D model preparation

The physical model of vertebrae with their internal structure was printed with the Ultimaker 3 printer (Ultimaker B.V., the Netherlands) in the FDM technology (Fused Deposition Modelling) which is one of the most often used additive manufacturing technologies of wires made of PLA (polylactic acid).

The vertebra digital model in a STL format was imported to the Ultimaker Cura 3D software. The printing parameters were selected from available options, such as a layer thickness, a filling structure, and a head speed. Next, the position and orientation of the model, which needed some support pillars, were fixed. This process was repeated several times until the acceptable configuration of the pillars was achieved, which would allow the model to be printed with the internal structure backed by the supporting material. A Gcode machine code was generated for the model to allow its printing on the 3D printer. The printer was equipped with two printing heads to print the model in two types of material. The elements of the vertebra model were printed in PLA, whereas the supporting elements were printed in water-soluble PVA. After printing, the elements were immersed in water for 24 h to dissolve the supporting material. Then, after rinsing, the model was left for 24 h to dry. Next, the prepared models were used in further investigations.

Experimental investigations

The test rig, configured for previous investigations where it had been verified as accurate and repeatable, was used [12]. A scheme of testing is presented in FIG. 2. The whole experimental system consisted of four main parts [12]. The first one, the Legato™210 infusion pump, was used as a cement flow generator, maintaining a constant given speed of the syringe plunger. A 10 cm³ capacity syringe made of acrylic glass was fixed in the infusion pump. The second part was an acrylic glass cannula connected to a pressure transducer via a pressure connector. The third piece, a glass cannula, served as a mechanical connection of the flow channel and the solid 3D vertebra model. Both cannulas had the same 3.0 mm internal diameter and were connected collinearly to minimize the flow disruption. Furthermore, they were transparent so as to observe the distribution of the flowing medium and to pinpoint the moment the cement began to flow into the vertebrae. Both cannulas were 72 mm long and the distance between the pressure tap and the model was 62 mm.

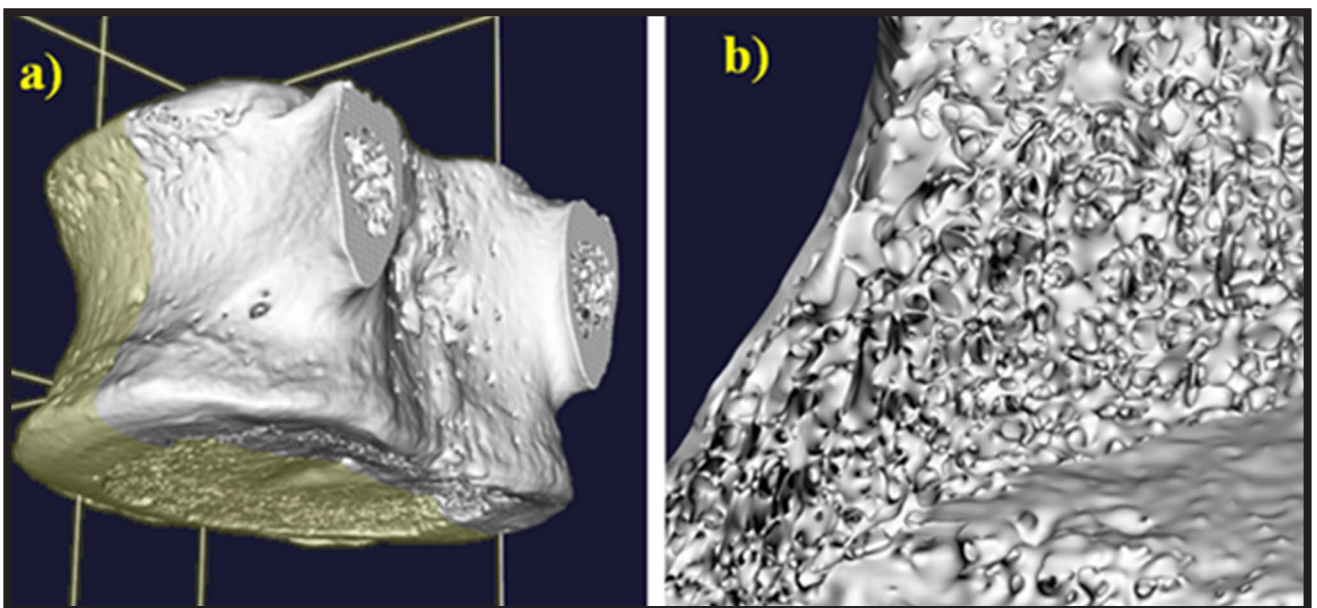


FIG. 1. View of a vertebra model: a) with planes indicating its cross-sections; b) visualization of the internal micro-architecture.

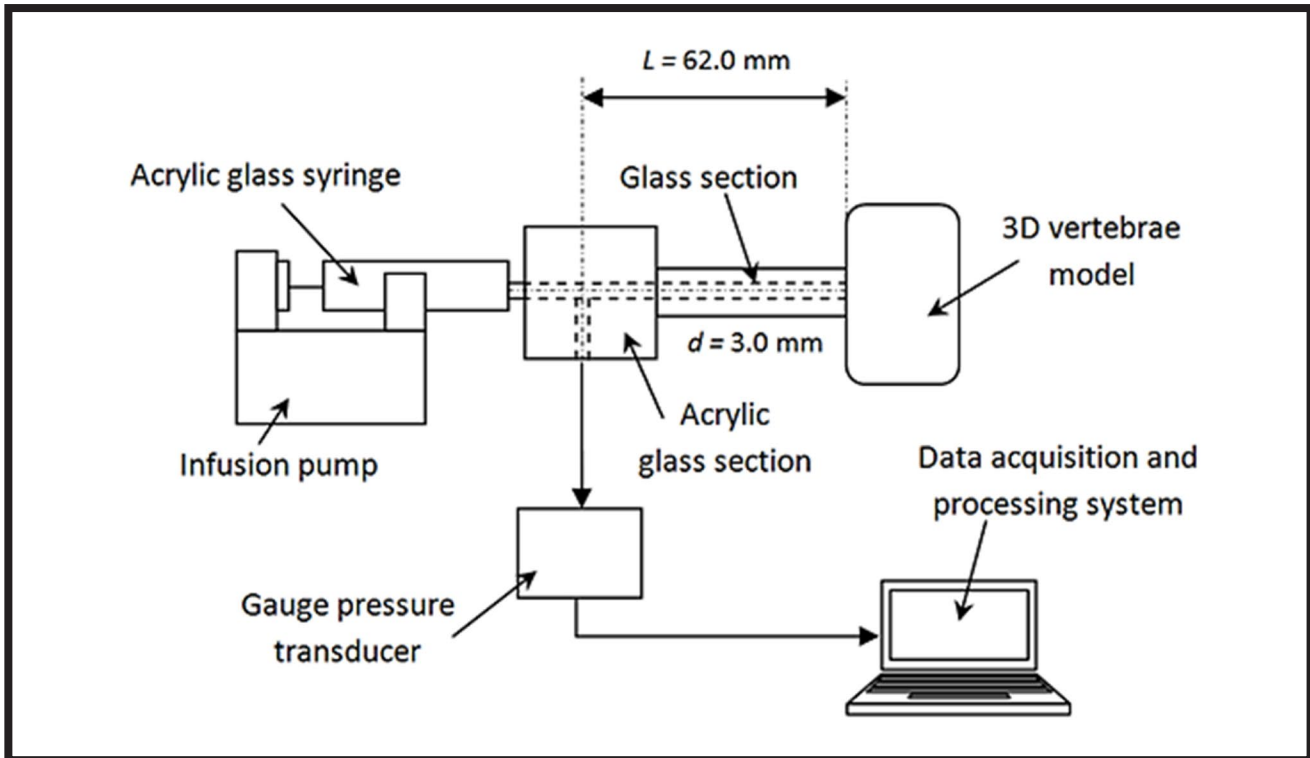


FIG. 2. Scheme of the test rig for investigations of the injection and distribution of bone cements in the 3D vertebra model.

Three models P1, P2, and P3 used in each trial were printed under the same conditions, from the same material, using the same 3D printer. The models resembled vertebrae with a weakened structure which needed to be supported by an implant, the bone or the cement, or both. In our case, the 3D printing of the bone structure was based on medical images, so we could claim that it correctly reproduced the porous bone structure in accordance with the Wolf's law. The change in bone density [28] affected the flow resistance of the cement inside the models. At the beginning of the tests, the flow channels in the model were filled with air. The glass cannula was inserted into a hole drilled in the vertebrae model. The tolerance of the cannula position was ± 1.8 mm horizontally and ± 0.6 mm vertically. The depth of the hole was 2.8 ± 0.1 mm in each case. To retain the connection tightness, the glass tube was pasted with the cyan acrylic glue.

According to the instruction provided by the producer, the mixing process of the bone cement components was maintained until the solid consistency mass was achieved, which did not take longer than 60 s. In the first trial, the cement was mixed carefully, limiting the number of press movements to 12 cycles. In the next trial, the cement was mixed at the speed advised by the producer, 24 cycles per minute, and in the third trial the number of cycles increased up to 32. The bone cement was injected into the vertebral body models. The flow speed was set to $1.0 \text{ cm}^3/\text{min}$ on the infusion pump (assuming an incompressible medium). To minimize the temperature influence on the experiment, all the trials were carried out in the laboratory where the temperature was $24 \pm 1^\circ\text{C}$. The cement flow was stopped in each trial when it started to flow out of the vertebrae model or when the entire volume of the prepared cement was administered. After the cement hardened, the samples were scanned with the CT scanner GE/LfC, with 0.074 mm definition. The reconstructed pictures of the vertebral bodies were used to evaluate the influence of aeration on the bone cement distribution in the specific models.

Results

The results were correlated and depicted in the pressure characteristics diagram as seen in FIG. 3. For every measurement, the time equal to 0 s referred to the beginning of the pump press movement.

There were characteristic points on each curve. The dashed vertical lines shown in the diagram corresponded to the moments when the cement crossed the feed channel and began to fill the vertebrae models. In all the cases, after filling the feed channel, there was the pressure increase resulting from the cement propagation in the stem model narrow channels (high local speed and increased resistance to movement). When the interior of the vertebrae model was filled with the reduced density, the pressure increase was lower. It can be concluded that this phenomenon was related to the vertebrae structure, whose thin structure in the center of the stem thickened towards the walls. As a result, the flow channels were narrower near the wall, resulting in the higher local velocity and the faster increase in pressure.

Despite the same flow rate set on the infusion pump, the course of the curves and the resulting cement delivery parameters differed on the case-by-case basis. The cement volume was also different. According to the indications of the infusion pump (for an incompressible fluid), the bone cement volume introduced through the system into the vertebral models was 7.0 , 7.4 , and 7.5 cm^3 , respectively. Using the CT data, the segmentation was performed and the bone cement volume inside the individual models was observed. The results are summarized in TABLE 1.

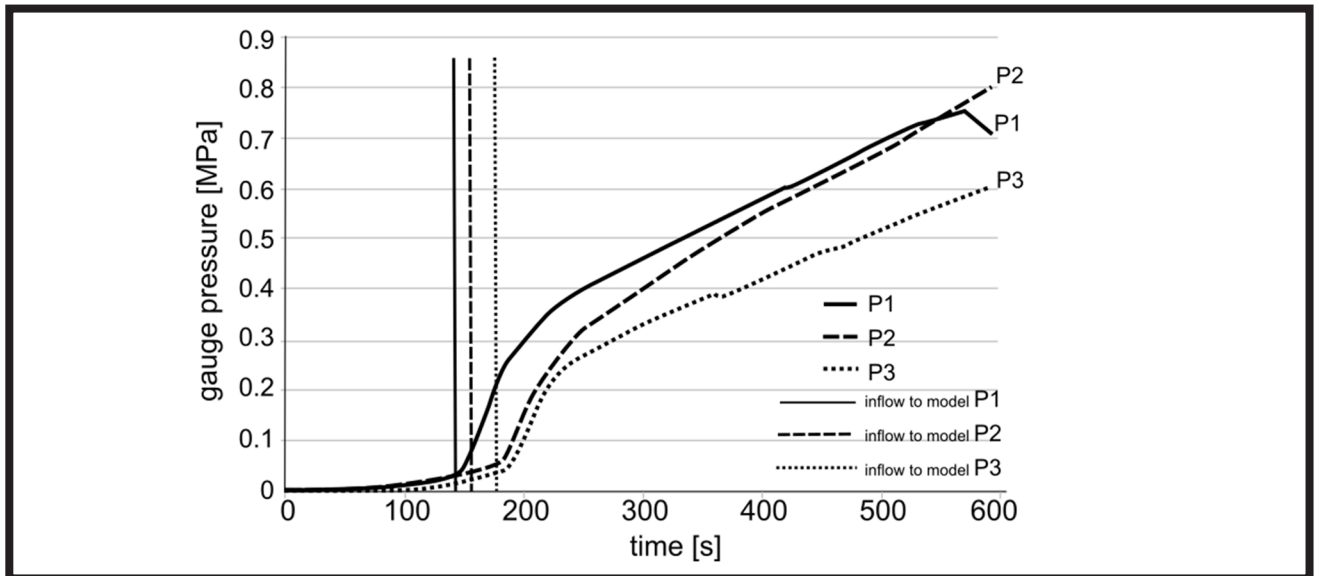


FIG. 3. Pressure characteristics acquired for every experimental case under analysis.

TABLE 1. Cement volume for vertebral bodies based on computer tomography.

Case	Total cement volume in the scanned sample [mm ³]	Cement volume inside the vertebral body [mm ³]
P1	5429.17	4602.41
P2	4877.17	4473.31
P3	2713.52	2525.62

Despite the same flow conditions and similar geometric conditions, the differences in the cement distribution can be seen in the CT scans (FIG. 4). In the first and second experiments, the cement filled the central space under the top border plate, the middle of the body and flowed into the left and right vertebral body walls. To some extent, it also filled the left side of the bottom body plate. In the third experiment, the cement filled the central space under the top boarder plate and the middle of the vertebral body. In the last case, the penetration had a much narrower range than in the previous two cases. In the third experiment, the cement did not fill the space above the top boarder plate. In every case, the cement tended to leak out through the anatomic foramen of the model back wall.

The transverse plane was used to provide the detailed distribution analysis for the five selected planes, according to the schemes presented in FIG. 5.

The results of the analysis were presented in a graphic form (FIG. 6) for the selected horizontal planes, every 4 mm, starting with the supply channel level to finish 3 mm below the boarder plate surface. The distribution in the central part surrounding the supply channel was rather regular for the 3 mm and 7 mm planes under the boarder plate. In the middle 11 mm plane, the medium flowed away in the direction of the anatomic foramen. For the 15 and 19 mm planes, the medium flowed into the front and the left body wall, which could be caused by the thinner vertebral body structure in this area.

In the microtomography images (FIG. 7) of the cross-section of the first sample P1, filled with the cement mixed with half the number of cycles, numerous air bubbles were observed. Air bubbles were found in the whole cement volume filling the vertebral body, as well as in the supply channel, where they clearly concentrated in its central area. In the second sample P2, filled with cement mixed with the number of cycles advised by the manufacturer, the quantity of air bubbles was lower in the vertebral body and in the supply channel. Air bubbles were smaller than those observed in the P1 sample. In the third sample P3, filled with the cement mixed with a higher number of cycles by half, large air bubbles were observed. The vertebral body filling was homogenous, and the cement filled numerous empty spaces in the body. There were longitudinal air bubbles in the cement in the supply channel.

Discussion

There were differences between the volume indications of the applied cement read from the infusion pump and the measurement results based on the TC scan. The reason for these differences was the fact that infusion pumps were to work with incompressible fluids, such as liquid medications, so they did not have a feedback loop. This phenomenon proved that the cement aeration should not be omitted during vertebroplasty procedures or while developing a mathematical model for the bone cement. Furthermore, the pump showed a given volume, although some cement was already lost to fill the supply channel.

The large number of small pores in the cement, especially in the cannula vicinity, showed that the cement could not be treated as a homogenous liquid. The high level of aeration may influence the cement further distribution. The numerous air bubbles in the flowing material may be constantly squeezed by pressure. As a result, the volume flow rate could significantly reduce in the further part of the channel.

All the above-mentioned differences (flow time, pressure characteristics, and a given volume) could stem from the three main factors: a random level of cement aeration, a difference in viscosity of the 3D printed models dependent on the printing time and precision. An influence of the temperature coming from a chemical reaction of cement with the 3D model structure should not be excluded either (glass transition temperature PLA 60-65°C).

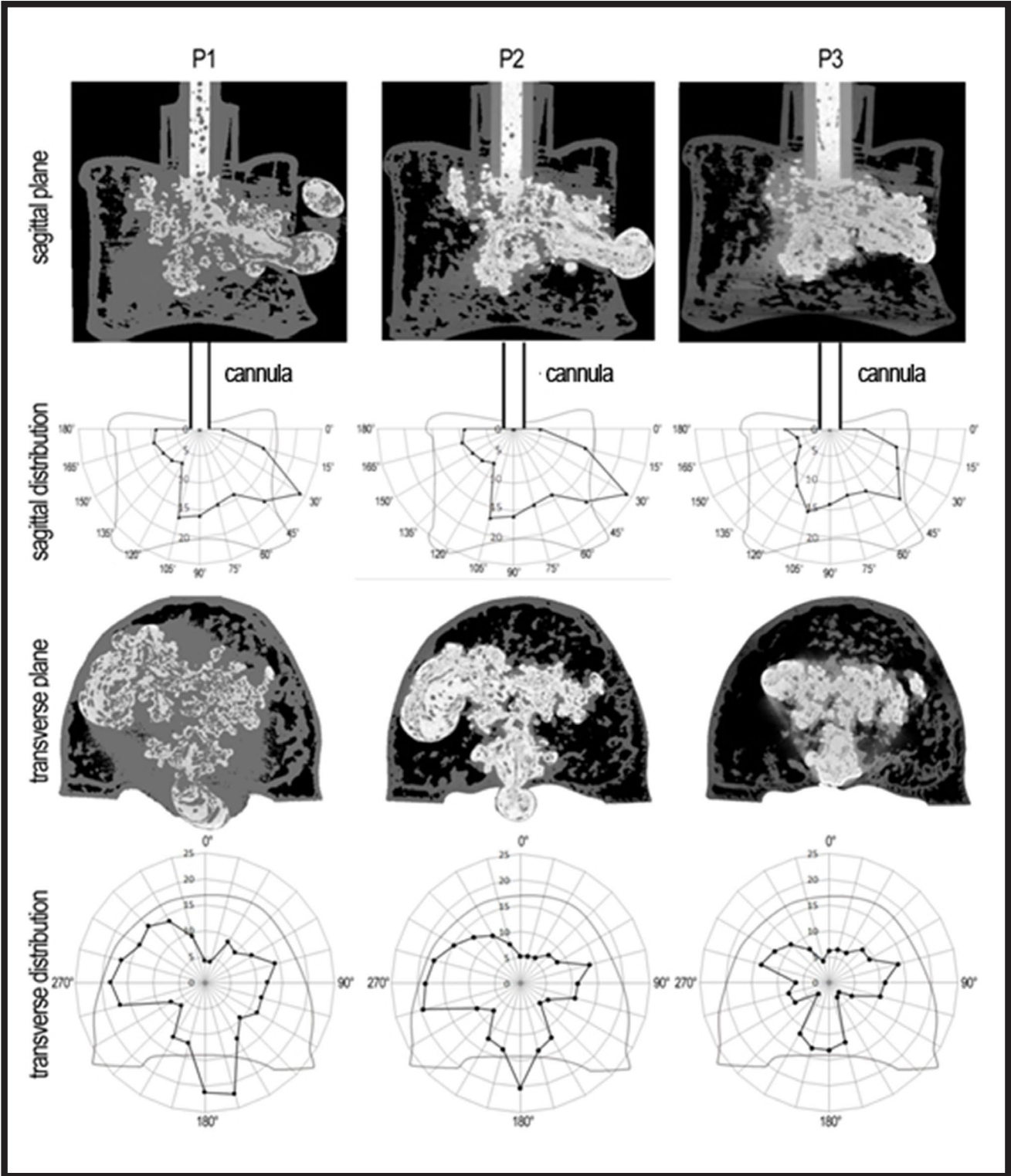


FIG. 4. Cement distribution in the sagittal plane through the vertebra center, and transverse plane for the middle slice (11 mm) of the vertebrae models for every case P1, P2 and P3 under analysis.

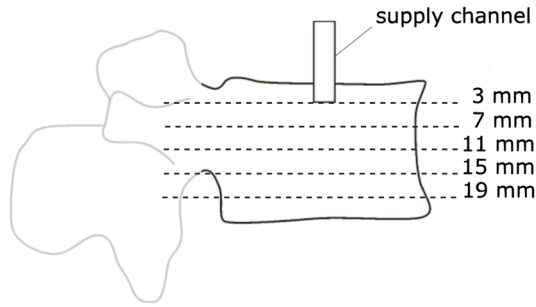


FIG. 5. Schematic view of the section position in the sagittal plane for evaluating the cement distribution.

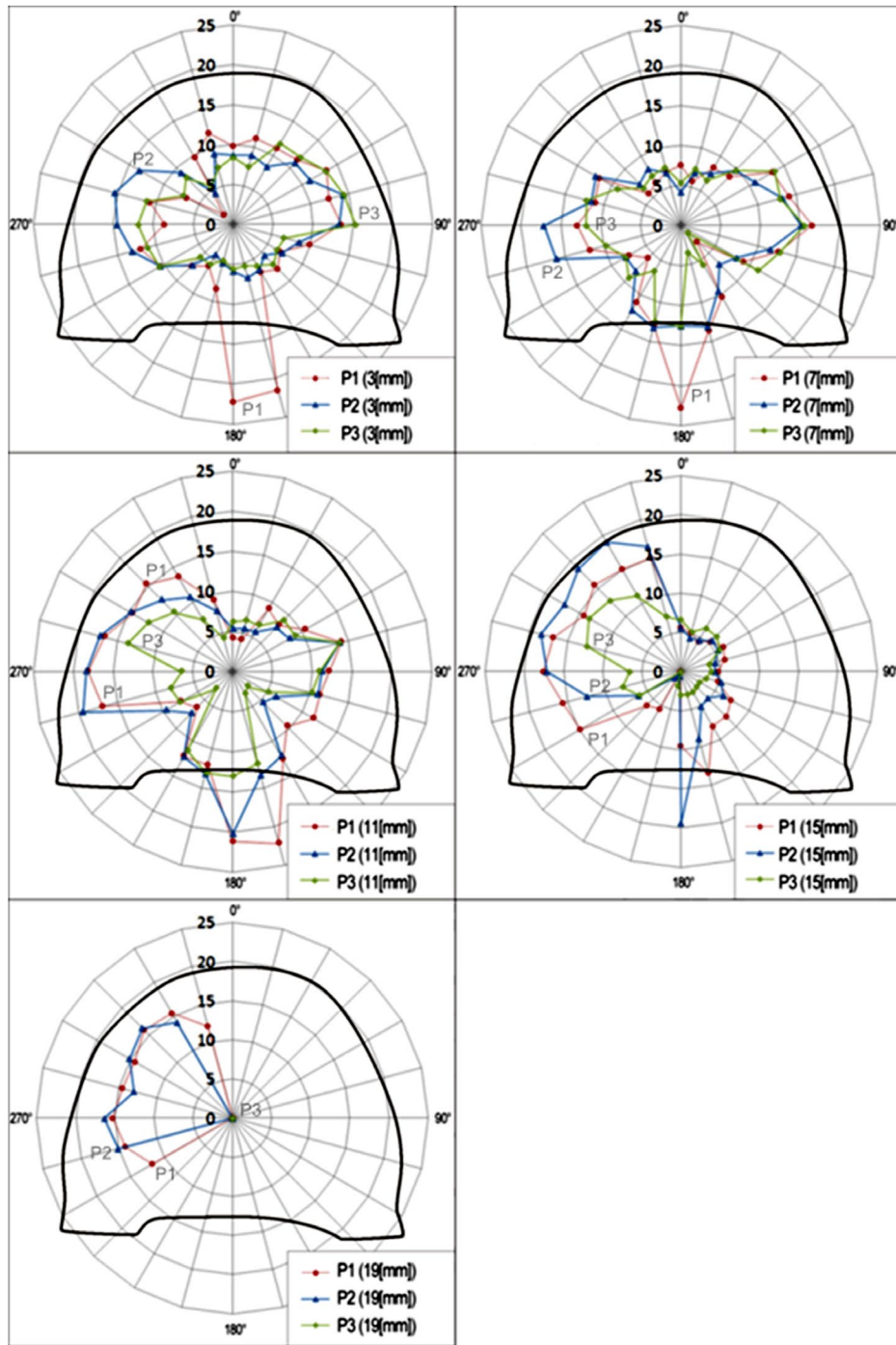


FIG. 6. Cement distribution in selected planes of the vertebral body models – the black contour.

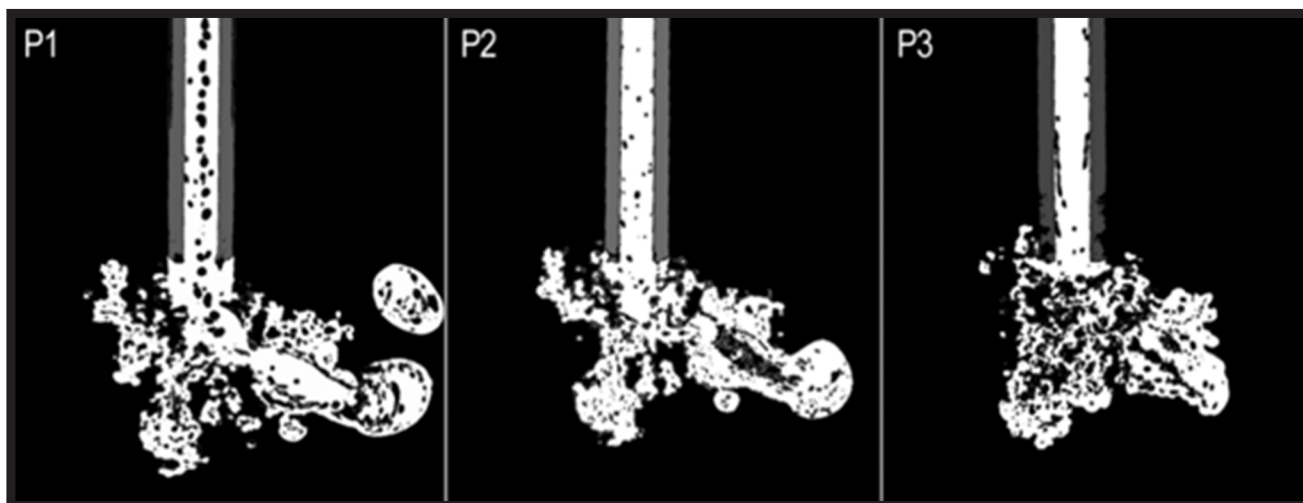


FIG. 7. Aerification of cement in the sagittal plane for every case under analysis.

Conclusions

The aerification level of bone cement had an important influence on the bone cement distribution in the vertebral body model. The low-aerified cement could penetrate well, which allowed the vertebral body to be filled evenly. The too high level of aerification lowered the penetration extent and influenced the homogeneity of the body being filled, which could influence its further biomechanical properties. The more precise interpretation requires further research in the field of aerification and the influence of its level on the medium distribution.

The tested models proved the 3D printing technique useful in the preparation of anatomical vertebral body models. However, the question remains whether the FDM resolution is sufficient or the SLA technology would be a better solution. The three-dimensional vertebral body models used in the experiments are easily accessible and inexpensive in comparison to the man-made unconsolidated preparations which are limited. Additional body models can be quickly replicated, which will enable further experiments to be conducted under comparable conditions.

Acknowledgements

The research was completed with the financial support of the National Centre for Research and Development in Poland (PBS3/B9/45/2015; within the project entitled: "Innovative medical surgical technology with implantable Inter Intra Vertebral body Fusion (IIVbF), expanding the effective treatment of degenerative spine", implemented in cooperation of the Lodz University of Technology, LfC, IBeMT and Bionanopark) and (POIR.01.01.01-00-0377/16; within the project entitled: "Multihybrid surgical technologies for treatment of aging spine; New spondyloimplantology spine" carried out by LfC Sp).

Declaration of Competing Interest

The authors declare that they have no known competing financial interests or personal relationships that could have appeared to influence the work reported in this paper.

ORCID iD

A. Bonik:	https://orcid.org/0000-0002-6094-2425
Z. Tyfa:	https://orcid.org/0000-0001-9870-8370
L. F. Ciupik:	https://orcid.org/0000-0002-8830-6965
K. Sobczak:	https://orcid.org/0000-0001-8994-6908
A. Kierzkowska:	https://orcid.org/0000-0003-3800-2733
D. Obidowski:	https://orcid.org/0000-0002-8950-6424
D. Witkowski:	https://orcid.org/0000-0003-4804-0266
T. Pałczyński:	https://orcid.org/0000-0002-2898-5302
M. Elgalal:	https://orcid.org/0000-0001-9127-0169
P. Komorowski:	https://orcid.org/0000-0002-4035-7501
E. Słowski:	https://orcid.org/0000-0001-7379-0128
K. Jóźwik:	https://orcid.org/0000-0002-7596-3691
B. Walkowiak:	https://orcid.org/0000-0003-4867-5456

References

- [1] Conference report. Consensus development conference: diagnosis, prophylaxis, and treatment of osteoporosis. *The American Journal of Medicine* 94 (1993) 646-650.
- [2] Hsuan-You Chen, Yen-Po Lin, Han-Ying Wang, Feng-Huei Lin, Po-Quang Chen, Ding-cheng Chan, Tze-Hong Wong, Ming-Hsiao Hu: Safer way for vertebroplasty under fluid mechanics theory. *The Spine Journal* 20 (2020) S77-S135.
- [3] Andrei D., Popa I., Brad S., Iancu A., Oprea M., Vasilian C., Poenaru D.V.: The variability of vertebral body volume and pain associated with osteoporotic vertebral fractures: conservative treatment versus percutaneous transpedicular vertebroplasty. *International Orthopaedics* 41 (2017) 963-968.
- [4] Adams M.A., Dolan P.: Perspective: Spine biomechanics. *Journal of Biomechanics* 38 (2005) 1972-1983.
- [5] Dengwei He, Chao Lou, Weiyang Yu, Kejun Zhu, Zhongwei Wu, Feijun Liu, Minjiang Chen, Lin Zheng, Zhenzhong Chen, Shunwu Fan: Cement distribution patterns are associated with recompression in cemented vertebrae after percutaneous vertebroplasty: a retrospective study. *World Neurosurgery* 120 (2018) e1-e7.
- [6] Bianciji E., Chiusa F., Pennati G.: Computational fluid dynamics of bone cement in procedures for osteoporosis treatment. 16th ESB Congress, Presentation, O154, S157.
- [7] Huber G., Muller-Bergen L., Heinze J., Eggers C., Purschel K., Morlock M.M.: Mechanical stability of augmented spinal segments. 5th World Congress of Biomechanics, München (2006).
- [8] Lin C-Y., Chuang S-Y., Ju D-T., Chen W-P.: Effects of bone stiffness, cement volumes and vertebral body height loss on the load transfer change of adjacent vertebrae in percutaneous vertebroplasty. *Journal of Biomechanics* 40 (2007) 584-585.
- [9] Wang J-L., Chiang Ch-K., Kuo Y-W., Chou W-K., Yang B-D.: Mechanism of fractures of adjacent and augmented vertebral following simulated vertebroplasty. *Journal of Biomechanics* 45 (2012) 1372-1378.
- [10] Jung Sik Bae, Heong Hyun Park, Ki Joon Kim, Hyeun Sung Kim, Il-Tae Jang: Analysis of risk factors for secondary new vertebral compression fracture following percutaneous vertebroplasty in patients with osteoporosis. *World Neurosurgery* 99 (2016) 387-394.
- [11] Tschirhart C.E., Roth S.E., Whyne C.M.: Biomechanical assessment of stability in the metastatic spine following percutaneous vertebroplasty: effects of cement distribution patterns and volume. *Journal of Biomechanics* 38 (2005) 1582-1590.
- [12] Tyfa Z., Witkowski D., Sobczak K., Obidowski D., Jóźwik K.: Experimental investigations of the aerated polymethylmethacrylate-based vertebral cement flow in capillaries. *The International Journal of Artificial Organs* 41(10) (2018) 670-676.
- [13] Race A., Mann K.A., Edin A.A.: Mechanics of bone/PMMA composite structures: An in vitro study of human vertebrae. *Journal of Biomechanics* 40 (2007) 1002-1010.
- [14] Tarsuslugil S.M., O'Hara R.M., Dunne N.J., Buchanan F.J., Orr J.F., Barton D.C., Wilcox R.K.: Development of calcium phosphate. *Journal of Biomechanics* 46 (2013) 711-715.
- [15] Kinzl E., Boger A., Zysset P.K., Pahr D.H.: The effects of bone and pore volume fraction on the mechanical properties of PMMA-bone biopsies extracted from augmented vertebrae. *Journal of Biomechanics* 44 (2011) 2732-2736.
- [16] Baroud G., Falk R., Crookshank M., Sponagel S., Steffen T.: Experimental and theoretical investigation of directional permeability of human vertebral cancellous bone for cement infiltration. *Journal of Biomechanics* 37 (2004) 189-196.
- [17] Boger A., Wheeler K., Montali A., Gruskin E.: NMP-modified PMMA bone cement with adapted mechanical and hardening properties for the use in cancellous bone augmentation. *Journal of Biomedical Materials Research Part B: Applied Biomaterials* 90(2) (2009) 760-766.
- [18] Kwon S.Y., Cho E.H., Kim S.S.: Preparation and characterization of bone cements incorporated with montmorillonite. *Journal of Biomedical Materials Research Part B: Applied Biomaterials* 83(1) (2007) 276-284.
- [19] Arabmotlagh M., Rickert M., Lukas A., Rauschmann M., Fleege Ch.: Small Cavity Creation in the vertebral body reduces the rate of cement leakage during vertebroplasty. *Journal of orthopaedic research* 35(1) (2017) 154-159.
- [20] Orlando O.A.: Vertebroplasty Cement Augmentation Technique. In: Razi A., Hershman S. (eds) *Vertebral Compression Fractures in Osteoporotic and Pathologic Bone*. Springer, Cham (2020) 115-135.
- [21] Furtos G., Tomoaia-Cotisel M., Baldea B., Prejmorean C.: Development and characterization of new AR glass fiber reinforced cements with potential medical applications. *J Appl Polym Sci*, 128(2) (2013) 1266-1273.
- [22] Furtos G., Tomoaia-Cotisel M., Garbo C., Şenilă M., Jumate N., Vida-Simiti I., Prejmorean C.: New composite bone cement based on hydroxyapatite and nanosilver. *Particul Sci Technol* 31(4) (2013) 392-398.
- [23] Barakat A.S., Alhashash M., Shousha M., Boehm H.: What an orthopaedic surgeon should know about vertebral cement augmentation. *Current Orthopaedic Practice* 28(4) (2017) 409-416.
- [24] Slane J., Vivanco J., Rose W., Ploeg H.L., Squire M.: Mechanical, material, and antimicrobial properties of acrylic bone cement impregnated with silver nanoparticles. *Materials Science and Engineering: C* 48 (2015) 188-196.
- [25] Farrar D.F., Rose J.: Rheological properties of PMMA bone cements during curing. *Biomaterials* 22(22) (2001) 3005-3013.
- [26] Spierlings P.T.: Properties of bone cement: testing and performance of bone cements. *The Well-Cemented Total Hip Arthroplasty: Theory and Practice*. Heidelberg: Springer Medizin Verlag Heidelberg (2005) 67-78.
- [27] Hernández L., Gurruchaga M., Goñi I.: Influence of powder particle size distribution on complex viscosity and other properties of acrylic bone cement for vertebroplasty and kyphoplasty. *Journal of Biomedical Materials Research, Part B: Applied Biomaterials* 77(1) (2006) 98-103.
- [28] Pietroń K., Mazurkiewicz Ł., Sybilski K., Małachowski J.: Correlation of Bone Material Model Using Voxel Mesh and Parametric Optimization. *Materials* 15(15) (2022) 5163.